12-1-2006

Geometric and Temperature Effects on Time Domain Reflectometry Measurements in Soils

Teresa Eileen Dallinger Ms
Purdue University

GEOMETRIC AND TEMPERATURE EFFECTS ON TIME DOMAIN REFLECTOMETRY MEASUREMENTS IN SOILS

A Thesis

Submitted to the Faculty

of

Purdue University

by

Teresa Eileen Dallinger

In Partial Fulfillment of the

Requirements for the Degree

of

Master of Science in Civil Engineering

December 2006

Purdue University

West Lafayette, Indiana

To Bonne Maman

ACKNOWLEDGMENTS

I would like to thank my advisor Professor Vincent P. Drnevich for his support and guidance throughout the research process. I would also like to extend my thanks to Professor Robert L. Nowack for his helpful suggestions and insight as well as to Professor Marika Santagata for fueling my interest in geotechnical engineering.

I am also grateful for the love and support of all of my family and friends. Although there are too many to list here, I would like to acknowledge the following people: Mom and Dad for allowing me to pursue my goals and interests; Bonne Maman for always believing in me; and of course a big thank you to Shelley and all of the long hours she spent with me at the Village Coffeehouse while I worked.

TABLE OF CONTENTS

Page

LIST OF TABLES

LIST OF FIGURES

Figure Page

Figure Page

ABSTRACT

Dallinger, Teresa Eileen. M.S.C.E., Purdue University, December, 2006. Geometric and Temperature Effects on Time Domain Reflectometry Measurements in Soils. Major Professor: Vincent P. Drnevich.

Time domain reflectometry (TDR) is a valuable tool used to measure the water content and dry density in soils. The success of TDR relies on the accurate measurements of the apparent dielectric constant (K_a) and the electrical conductivity (EC_b). This study focuses on improving TDR measurements. The measured electrical conductivity is related to the geometry of the electromagnetic field which is a function of the probe design. The most important factors that define the field are the number, locations, and dimensions of the inner and outer conductors. An investigation of the influence of the probe head geometry on EC_b is performed using groundwater modeling techniques. Finite difference and finite element models are created for different probe configurations used both in the field and in the laboratory and recommendations are made to correct the d.c. electrical conductivity measured in time domain reflectometry for different probe geometries. Temperature effects on K_a and EC_b measurements in soils as well as the pulse area of the first and second reflections of the TDR waveform are also analyzed. Test results on compacted soils show that in cohesive soils the apparent dielectric constant increases with increasing temperatures, while it decreases with increasing temperature in non-cohesive soils. The electrical conductivity measurements are significantly more affected by temperature changes than the apparent dielectric constant; however, the trend appears to be relatively independent of soil type and texture. In both cohesive and non-cohesive soils, the electrical conductivity was observed to increases as the temperature increases. Both pulse areas decrease as the temperature increases;

however, the pulse area of the second reflection shows a greater variation with temperature than the pulse area of the first reflection. Recommendations are made to correct measured values of the apparent dielectric constant, electrical conductivity, and pulse areas to values at 20°C.

CHAPTER 1. INTRODUCTION

1.1. Statement of the Problem

Time domain reflectometry (TDR) is a technique used to measure the dielectric properties of soils, specifically the apparent dielectric constant, K_a and the electrical conductivity, EC_b. Siddiqui and Drnevich (1995) and Yu (2003) developed empirical equations relating these two parameters to the water content and dry density of the soils. The accuracy of the estimation of water content and dry density relies on the measurement of K_a and EC_b.

The focus of this investigation is to improve the accuracy of the TDR method for measuring water content and dry density. A number of factors can affect TDR measurements including porosity, soil specific surface area, geometric arrangement of particles, temperature, and geometry of the TDR probe head (Robinson et al., 2006, Wraith and Or, 1999, Robinson et al., 2003). This study concentrates on two of these factors. Different probe head geometries are evaluated in order to determine appropriate geometric correction factors for the electrical conductivity measurements. Corrections to measurements of K_a and EC_b due to fluctuations in temperature are also recommended.

1.2. Objectives

The main objectives of this study include:

1. Evaluate the effects of the TDR probe head geometry on the estimation of the electrical conductivity and propose new correction factors, if necessary.

2. Investigate the variation of the apparent dielectric constant and the electrical conductivity with temperature and propose new correction factors, if necessary.

3. Analyze the effects of temperature on the pulse area of the TDR waveform and propose correction factors, if necessary.

1.3. Organization

Chapter 2 summarizes the investigation of different TDR probe geometries using groundwater flow models to predict the geometric factors needed to accurately estimate the electrical conductivity of soils. Updated corrections based on this analysis are presented.

The temperature effects on the TDR measured apparent dielectric constant and electrical conductivity of soils are investigated in Chapter 3 and Chapter 4, respectively. The results are compared to previous studies which are summarized in the first section of this chapter.

Chapter 5 investigates the temperature effects on the pulse area of the TDR waveform. The pulse area is a relatively new measurement that with the apparent dielectric constant and electrical conductivity may be able to more accurately predict the water content and dry density of soils. Chapter 6 provides a summary of the conclusions and recommendations.

CHAPTER 2. INFLUENCE OF TIME DOMAIN REFLECTOMETRY HEAD GEOMETRY ON THE ELECTRICAL CONDUCTIVITY DETERMINATION

2.1. Introduction

The electrical conductivity (EC_b) is a material property of soils that can be measured using time domain reflectometry (TDR). EC_b is an important property that can be used to estimate the water content and dry density of soils. It can also be an indication of soil salinity in the field (Rhodes et al., 1976). However, there are often inconsistencies in lab measurements and those measured in the field. TDR measurements are influenced by the geometry of the probe (Robinson et al., 2003) which could explain some of the discrepancies in measurements between lab and field measurements since the probe head used in the laboratory has a different geometry than the probe head used in the field.

The measured electrical conductivity is related to the geometry of the electromagnetic field and this is a function of the probe design. The most important factors that define the electromagnetic field are the location and dimension of the inner and outer conductors. Laboratory testing is commonly performed using standard compaction molds. These molds act as the outer conductor and provide a continuous outer boundary for the electromagnetic field. The inner conductor is a center spike, driven into the material. In contrast, measurements in the field involve multiple rod probes with 2, 3, 4, or more rods inserted into the soil. The work done at Purdue uses a 4 rod configuration, a center rod and 3 outer rods equally spaced at the same radius from the center. Instead of a continuous outer boundary the electromagnetic field consists of 3 sinks for the energy to flow towards. The different electromagnetic fields generated by these different geometric configurations could affect the flow of energy between the conductors. Modeling of the electromagnetic fields can help determine the effects of the probe design on the measurements of electrical conductivity.

The remaining part of this chapter will investigate the different probe geometries used both in the laboratory and in the field. By altering the geometric factors used to calculate EC_b, more accurate measurements can be made for better consistency between laboratory and field measurements.

2.2. Evaluation of Electrical Conductivity

The electrical conductivity can be obtained from the long term response of a TDR system. Giese and Tiemann (1975) first explored the possibility of directly interpreting the waveform of thin samples. Topp et al. (1990) applied the approach to measuring electrical conductivity in soils and found the results satisfactory. Yu (2003) further investigated transmission line theory and made use of the expression by Giese and Tieman (1975) for the electrical conductivity based on the steady state response, as

$$EC_b = \frac{1}{C}\left(\frac{V_s}{V_f} - 1\right) \qquad \text{Eq. 2.1}$$

where V_s is the source voltage, V_f is the final or long term voltage (Figure 2-1) and C is a constant related to the probe geometry and the TDR pulse generator. For a coaxial probe configuration

$$C = \frac{2\pi \cdot L \cdot R_s}{\ln\left(\frac{R}{r}\right)} \qquad \text{Eq. 2.2}$$

where R_s is the resistance of the pulse generator, L is the length of the probe in the soil, R is the radius of the outer conductor and r is the radius of the inner conductor.

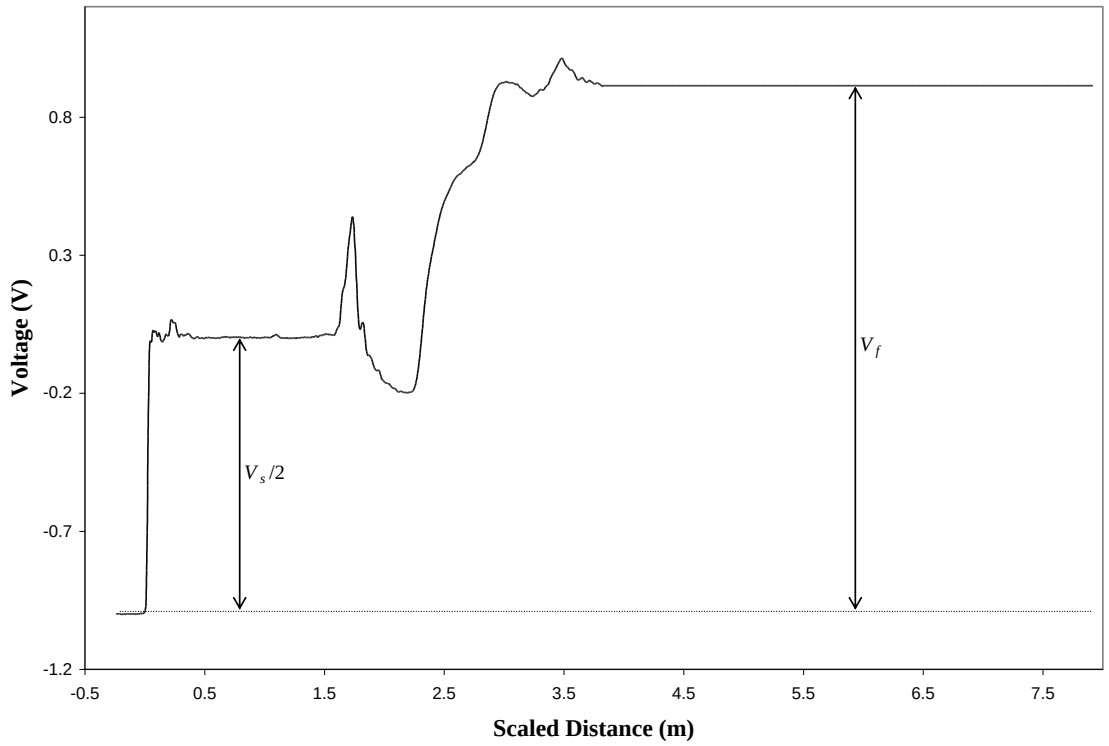

Figure 2-1 TDR waveform for fine sand, water content = 20%, V_s is the source voltage, and V_f is the final voltage

Equation 2.2 provides a good estimation for the geometric factor for coaxial configurations, but does not directly apply to a 4 rod field probe. The outer conductors for this configuration are 3 rods spaced at a distance from the center rod, which do not form a continuous boundary. Despite this, the same constant C is currently being used (ASTM D6780) to calculate the electrical conductivity of soils regardless of the difference in probe geometry leading to discrepancies between field and laboratory measurements. More accurate values of C are needed to account for the differences in probe configuration.

2.2.1. Electric Flow and Groundwater Flow

Mualem and Friedman (1991) proposed a conceptual model for predicting the electrical conductivity of saturated and unsaturated soils. Their model was based on the similarity between electrical and groundwater flow. The assumption is that the flow lines of water molecules in soil under a hydraulic gradient are similar to the flow lines of the electric current in the same soil under electrical potential gradient. Therefore, the same geometry factor used in groundwater flow can be applied to electric flow. With this assumption, groundwater flow models can be used to simulate the flow of electricity through the soil. The models can predict the rate of flow of electricity which can provide information regarding the dissipation rate for a given probe configuration.

The two-dimensional flow of water through homogeneous and isotropic soils can be represented by the Laplace equation for total hydraulic head.

$$\frac{\partial^2 h}{\partial x^2} + \frac{\partial^2 h}{\partial z^2} = 0 \qquad \text{Eq. 2.3}$$

where h is the hydraulic head.

Equation 2.3 can be illustrated with a flow network constructed from equipotential and flow lines. The equipotential lines represent the lines along which water can flow through the cross-section. The equipotential lines are lines of equal total head. Flow lines intersect the equipotential lines at right angles to form square areas defined by the average width of the area is equal to the average length of the area. An important property of flow networks is the shape factor which is equal to the ratio of the number of flow channels (n_f) to number of head drops (n_d). Properly constructed flow networks for a given set of conditions have approximately the same shape factor regardless of the number of flow lines and equipotential lines drawn. Hand drawn flow networks can provide approximations to the groundwater flow behavior and solutions to the Laplace equation. However, numerical models and computer software programs have been created to analyze more complex situations.

The shape factor of a flow network depends on the geometry of the system. A portion of the definition of the constant *C* used to calculate the electrical conductivity is related to the probe configuration and the rest is a function of the pulse generator. A new constant solely dependent on the geometry *C'* can be defined by:

$$C' = \frac{2\pi}{\ln\left(\frac{R}{r}\right)} \qquad \text{Eq. 2.4}$$

C' is obtained by neglecting the influence of the length of the probe into soil (*L*) and the resistance of the pulse generator (R_s). The influence of length of the probe is removed because the analysis is based on a two-dimensional plan view of the horizontal flow of electricity through the soil. *C'* is considered as the two-dimensional shape factor for the electrical flow through the system and is assumed to be analogous to the shape factor for groundwater flow, where

$$\frac{n_f}{n_d} = C' = \frac{2\pi}{\ln\left(\frac{R}{r}\right)} \qquad \text{Eq. 2.5}$$

It is then possible to use groundwater flow models to find the shape factor and compute appropriate values of *C* for different probe configurations.

2.3. Analysis

Two numerical models used for groundwater flow are the finite difference method and finite element method. Each provides the approximate location of the equipotential lines by creating a mesh within the area to be analyzed and calculating the hydraulic head differences at each node of the mesh. The finite difference method is a more crude approximation which uses only rectangular meshes. The finite element method is able to use triangular in addition to rectangular meshes. These two methods were used to analyze the different probe configurations used in field and laboratory testing.

Three different geometries were analyzed using both the finite difference and finite element methods:

- 5/16” diameter center spike with a 4” diameter cylinder
- 3/8” diameter center spike with a 6” diameter cylinder
- 3/8” diameter center spike with 3-3/8” diameter spikes located 2.588” from the center spike 120 degrees apart

Two additional geometries were analyzed using only the finite element method:

- 3/8” diameter center spike with 3-3/8” diameter spikes located 2.588” from the center spike 120 degrees apart inside a 6” diameter cylinder
- 3/8” diameter center spike with 3-3/8” diameter spikes located 2.588” from the center spike 120 degrees apart inside an 11” diameter cylinder

Due to the symmetry of the problems, 60 degree wedges were used to limit the size of the models. Because the models are $1/6^{th}$ the size of the actual configuration, the number of flow channels in the model are multiplied by 6 to obtain the overall number of flow channels for the system.

2.3.1. Finite Difference Method

The basic principle is to replace the partial derivatives in the Laplace equation with finite differences to obtain an approximate numerical solution. The cross section is divided into a finite number of rectangles of width Δx and length Δy (Figure 2-2). By assuming that $\Delta x = \Delta y$, an approximate solution to equation 2.3 can be found using forward and backward derivative estimations. Equation 2.6 can be used to compute the total head for any node A, not located along an impervious boundary.

$$h(x_a, y_a) = \frac{1}{4}(h(x_a, y_a + \Delta y) + h(x_a, y_a - \Delta y) + h(x_a + \Delta x, y_a) + h(x_a - \Delta x, y_a)) \quad \text{Eq. 2.6}$$

Equation 2.7 is the modified equation used at points which occur along an impervious boundary (point B).

$$h(x_b, y_b) = \frac{1}{4}(h(x_b, y_b + \Delta y) + h(x_b, y_b - \Delta y) + 2 \cdot h(x_b + \Delta x, y_b)) \quad \text{Eq. 2.7}$$

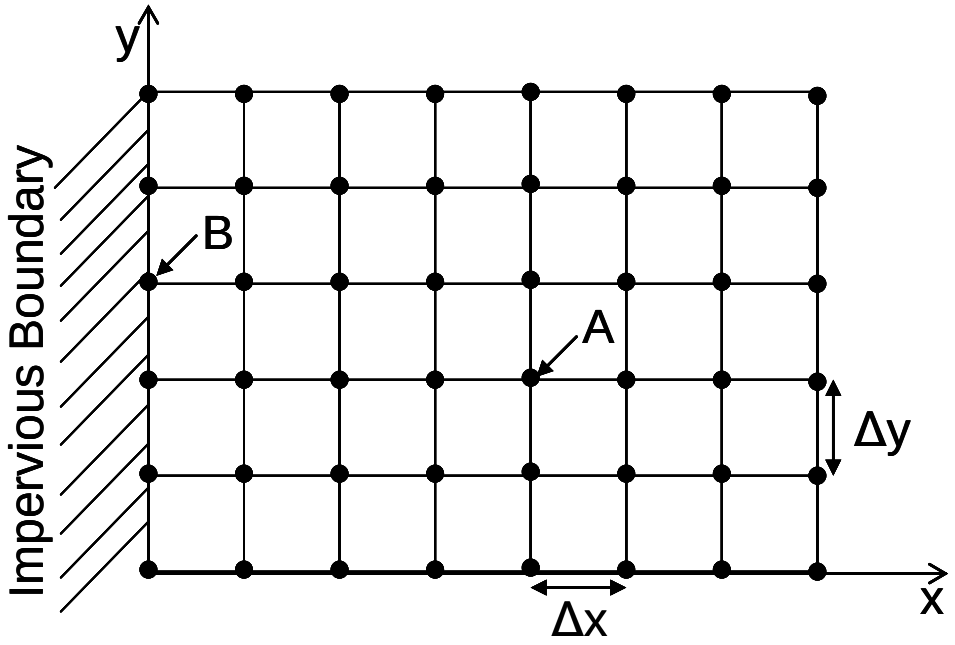

Figure 2-2 Finite difference method mesh

Plots of the equipotential lines were created by programming the equations into a Microsoft Excel spreadsheet. Sketches of the geometries were made in order to identify the 60 degree boundary. The nodes nearest to the line drawn as the boundary were chosen as the approximate boundary for the wedge. The same is true for the boundary created by the cylinder. One of the disadvantages to the finite difference method is that infinite boundaries cannot be easily modeled. The field probe configuration only has three outer rods to provide the boundary conditions. A fictitious zero head boundary needed to be imposed at a sufficient distance to limit the effects on the head loss in the system. A comparison of plots with the boundary located at 4" and 5.2" from the center spike showed little difference in the head losses, therefore 4" was chosen for the location of the imposed zero head boundary.

In order for energy to flow through the system a potential difference between two points is necessary. The center spike is the source of the electromagnetic pulse which flows through the soil to the outer boundaries. To simulate this, a hydraulic head 100 inches (electric potential of 100 Volts) was assigned to nodes representing the center spike and a 0 inch hydraulic head (0 Volt potential) to the nodes representing the cylinder and outer spikes. The initial mesh spacing was 0.05 inch. A second mesh with a smaller spacing, 0.025 inch was also created to observe the effects of using a finer mesh. Contour plots were created by grouping the calculated head values at each node. The resulting equipotential lines represent 10 inches of hydraulic head loss (10 Volts of potential loss). Plots of the equipotential lines for the 4 inch cylinder show that most of the potential loss occurs close to the center spike (Figure 2-3 and Figure 2-4). Figure 2-4 represents the same configuration analyzed using a finer mesh. Some changes did occur in the region closest to the center spike. Figure 2-5 shows a close up of the first 0.5 inch from the center spike using an even finer mesh in this sensitive area.

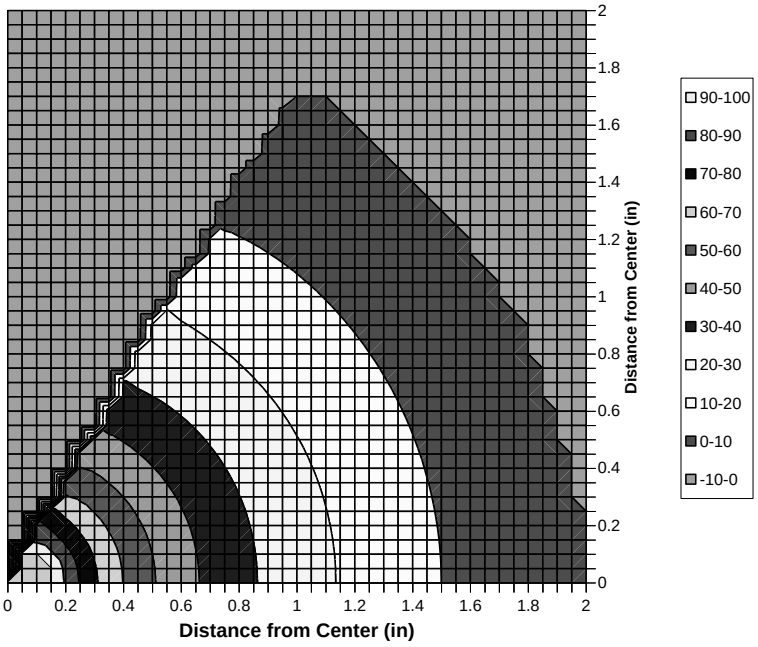

Figure 2-3 Equipotential contours, each representing 10 inches of hydraulic head loss (10 Volts of potential loss), for a 5/16 inch diameter center spike inside a 4 inch diameter cylinder using a 0.05 inch mesh spacing

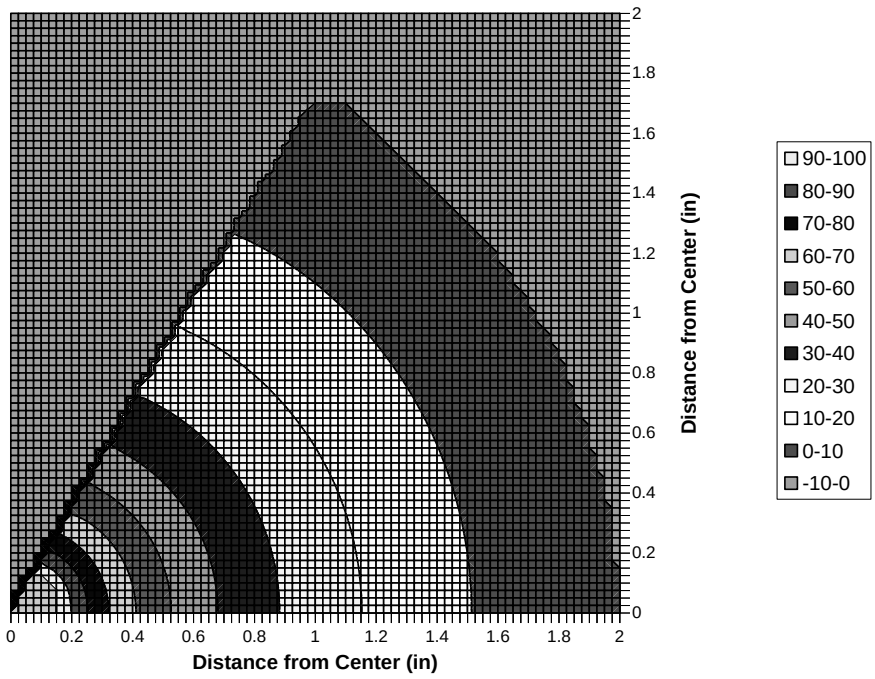

Figure 2-4 Equipotential contours, each representing 10 inches of hydraulic head loss (10 Volts of potential loss), for a 5/16 inch diameter center spike inside a 4 inch diameter cylinder using a 0.025 inch mesh spacing

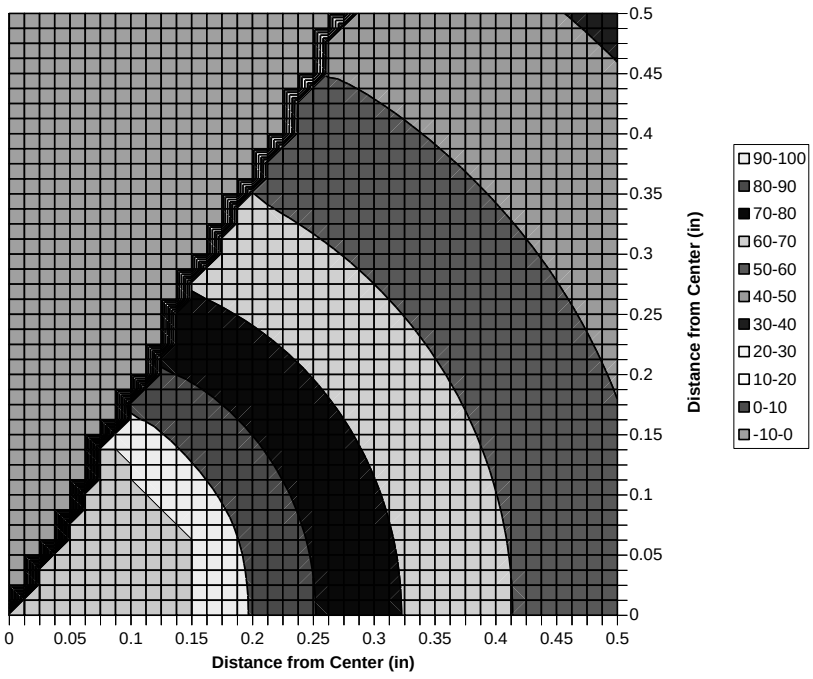

Figure 2-5 Equipotential contours, each representing 10 inches of hydraulic head loss (10 Volts of potential loss), for a 5/16 inch diameter center spike inside a 4 inch diameter cylinder using 0.0125 inch mesh spacing from 0 to 0.5 inches from the center and 0.025 inch mesh spacing for the remainder

For determination of the number of flow channels for the wedge, flow lines were drawn on the plots by measuring the distance between two equipotential lines and creating squares in that zone. This number was then multiplied by 6 to obtain the total number of flow channels for the system.

2.3.2. Finite Element Method

The finite element method is based on the concept of subdividing the system into small elements, analyzing the behavior of each element, then reconnecting the elements to represent the behavior of the entire system. Similar to the finite difference method, there are nodes at each corner of the elements. Due to the number and complexity of the equations involved, this method relies on computer software for efficient implementation.

This investigation utilized the SEEP/W program which is a subset of the GeoStudio 2004 software package.

There are three fundamental aspects to modeling using finite element analysis. The first is the creation of a mesh of finite elements (meshing), the second is the identification of the material properties and third is the boundary conditions. Meshing is the process of subdividing the area of interest into elements to be analyzed by the software program. SEEP/W features two different types of meshes, structured and unstructured. Structured meshes are composed of quadrilateral shaped elements ordered in a consistent pattern. Unstructured meshes are created using Delaunay triangular techniques and feature triangular shaped elements. The elements are most effective when they are closest to the ideal shape, squares for quadrilaterals and equilateral or isosceles right triangles. In general, quadrilateral elements offer better behavior than triangular elements. However, for simple seepage analysis, triangular elements perform adequately. The advantage to using an unstructured mesh is that it can be used to model irregular geometries. For tight spaces it is difficult to produce ideal meshes of quadrilateral elements, therefore triangular unstructured meshes are more appropriate. For this reason, a mesh of triangular unstructured elements was used for the area close to the center spike. This mesh is also more refined close to the center which as observed during the finite difference analysis is where a majority of the head loss occurs. The rest of the wedge used a structured mesh. Figure 2-6 shows an example of the mesh used for analysis.

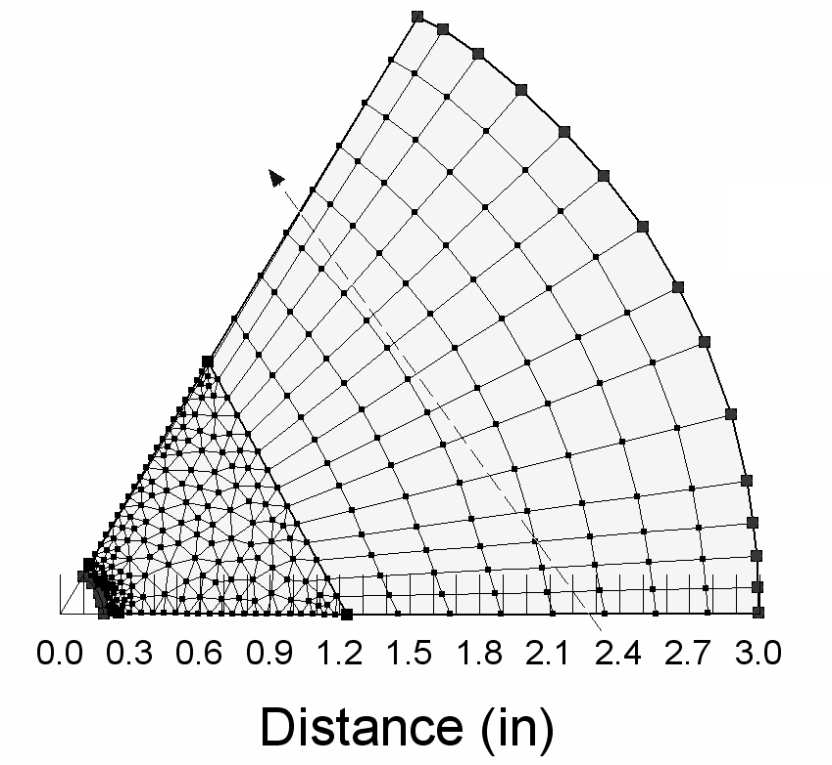

Figure 2-6 Finite element mesh for a 3/8 inch diameter center spike inside of a 6 inch diameter cylinder produced by SEEP/W

An approximate value of the hydraulic conductivity is required for analysis using the SEEP/W program. The goal of this evaluation is to find the shape factor of the system, which is a geometric property and is independent of the hydraulic (electrical) conductivity. For the purposes of this investigation the hydraulic conductivity was defined as 1 in/s (electrical conductivity 1V/s).

The boundary conditions define the flow through the system. A difference in energy is required for flow to occur. A hydraulic head of 100 inches (electric potential of 100 Volts) was assigned to the nodes located along the edge of the center spike and 0 inches (0 Volts) was assigned to nodes along the edges of the outer spikes and the cylinders. Contour plots of the resulting equipotential representing 10 inches of head loss (10 Volts of potential loss) were created and the flow rate through the section was

reported (Figure 2-7). Because the model is 1/6th the size of the actual configuration the flow rate needs to be multiplied by 6 in order to obtain the overall flow rate in the system.

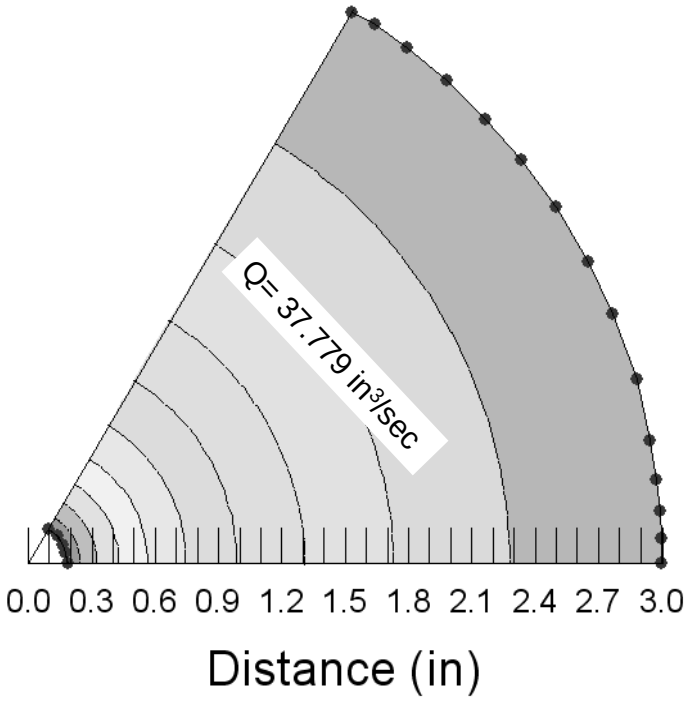

Figure 2-7 Equipotential contours, each representing 10 inches of hydraulic head loss (10 Volts of potential loss) for a 3/8 inch diameter center spike inside of a 6 inch diameter cylinder

One advantage to the finite element method is that the flow rate through the system can be directly calculated. Therefore, instead of plotting equipotential lines and trying to draw the flow lines manually, the shape factor can be determined from the flow rate. The flow rate, q is defined by:

$$q = k\Delta H \frac{n_f}{n_d} \qquad \text{Eq. 2.8}$$

where k is the hydraulic (electrical) conductivity, ΔH is the total difference in energy between the boundaries and n_f/n_d is the shape factor. Thus, solving for the shape factor,

$$\frac{n_f}{n_d} = \frac{q}{k\Delta H} \qquad \text{Eq. 2.9}$$

Note that the flow rate reported by SEEP/W is the volumetric flow rate. The analysis assumes that the depth of the model is equal to 1 inch.

Another advantage to using the finite element method is that semi-infinite boundaries (boundaries without conditions) can be modeled using the SEEP/W program. The finite difference method required the use of an imposed zero head boundary for analysis. The ability to easily change the boundary conditions allowed for an investigation of the effects of the imposed zero head boundary using finite element analysis. The contour plots show that the imposed zero head boundary distorts the equipotential lines, especially those close to the outer spikes. The flow rate is also larger when the boundary is imposed on the system.

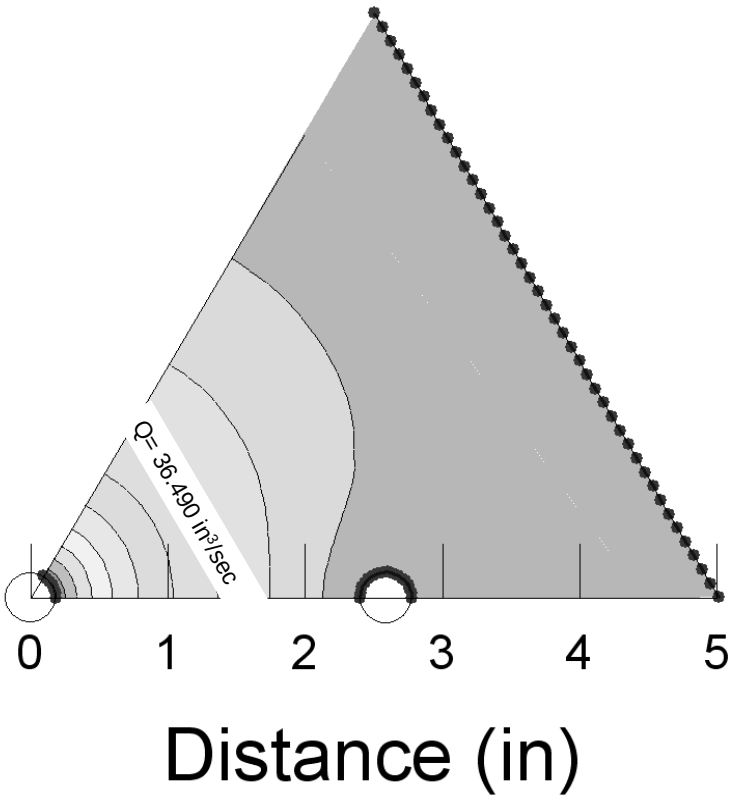

Figure 2-8 Equipotential contours, each representing 10 inches of hydraulic head loss (10 Volts of potential loss), for a 3/8 inch diameter center spike with 3/8 inch diameter outer spikes located 2.588 inch from the center spike with an imposed zero head boundary at 5 inches

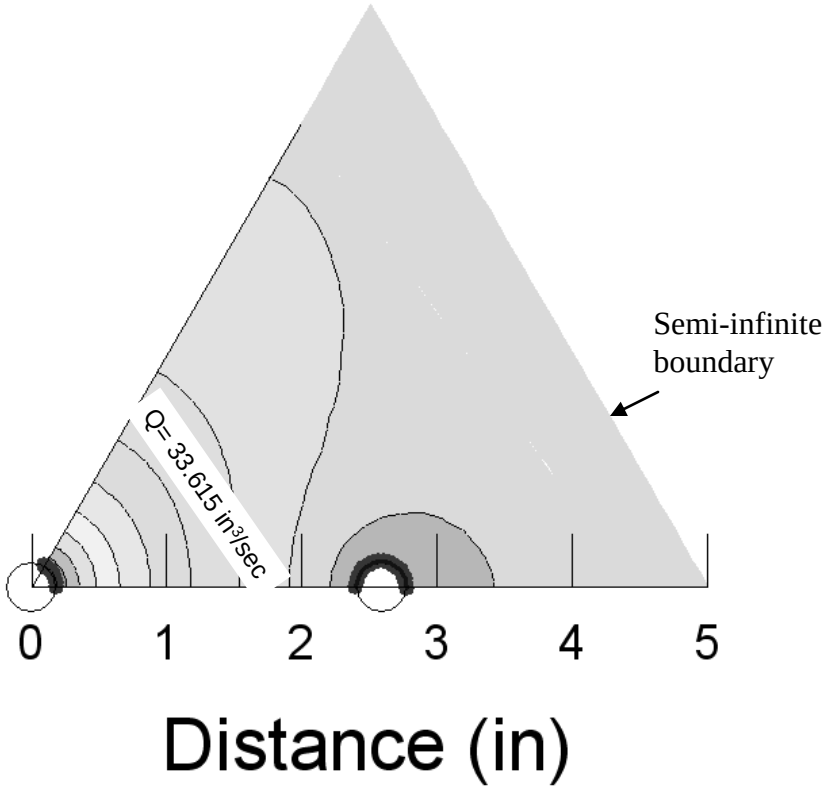

Figure 2-9 Equipotential contours, each representing 10 inches of hydraulic head loss (10 Volts of potential loss), for a 3/8 inch diameter center spike with 3/8 inch diameter outer spikes located 2.588 inch from the center spike with a semi-infinite boundary

In reality there is no outer boundary to the electric field for the field probe configuration. Therefore the semi-infinite boundary is a more accurate representation of the conditions. This is confirmed by the analysis of the electromagnetic field obtained by Zambrano (2006) using Ansoft Maxwell® 2D field solver (2005) shown in Figure 2-10. The model was analyzed multiple times by moving the semi-infinite boundary to different distances from the center spike. The boundary was drawn as a straight line with one point on the x-axis and a second point on the 60 degree line, both points equal distance from the center of the center spike. The boundary was also drawn as an arc with constant radius. In both cases similar results were obtained for semi-infinite boundaries located 5 inches to 30 inches from the center spike. SEEP/W also allows the use of

infinite elements to simulate an infinite boundary using a built-in decay function to calculate the flow and head loss. Analysis using the semi-infinite boundary and the infinite elements yielded the same results.

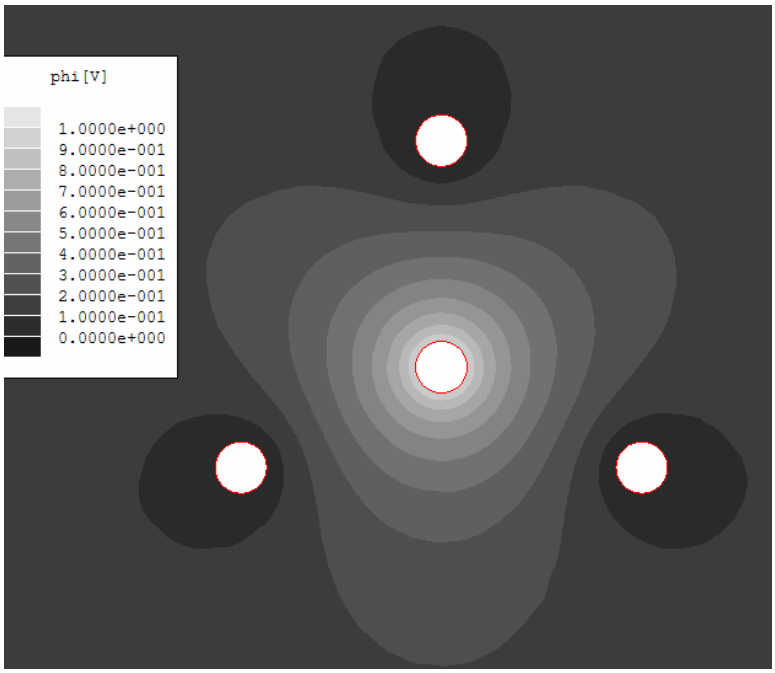

Figure 2-10 Voltage distribution in field multiple rod probes obtained with Ansoft Maxwell® 2D field solver (2005) from Zambrano (2006)

2.4. Two and Three Rod Probes

Coaxial probe configurations are common to the Purdue TDR Method. However they are not the only type of probe available. Two and three rod probes are also a common probe configurations used to measure the apparent dielectric constant and electrical conductivity in soils. The finite element method was used to evaluate each of these probes in a similar manner to the configurations previously discussed.

The two rod probe consists of two rods 2.5 millimeters in diameter spaced 20 millimeters apart. One rod was assigned a hydraulic head of 100 millimeters (100 Volts) and the other rod was assigned a hydraulic head of 0 millimeters (0 Volts). Contour plots

of the resulting equipotential representing 10 inches of head loss (10 Volts of potential loss) were created and the flow rate through the section was reported (Figure 2-11).

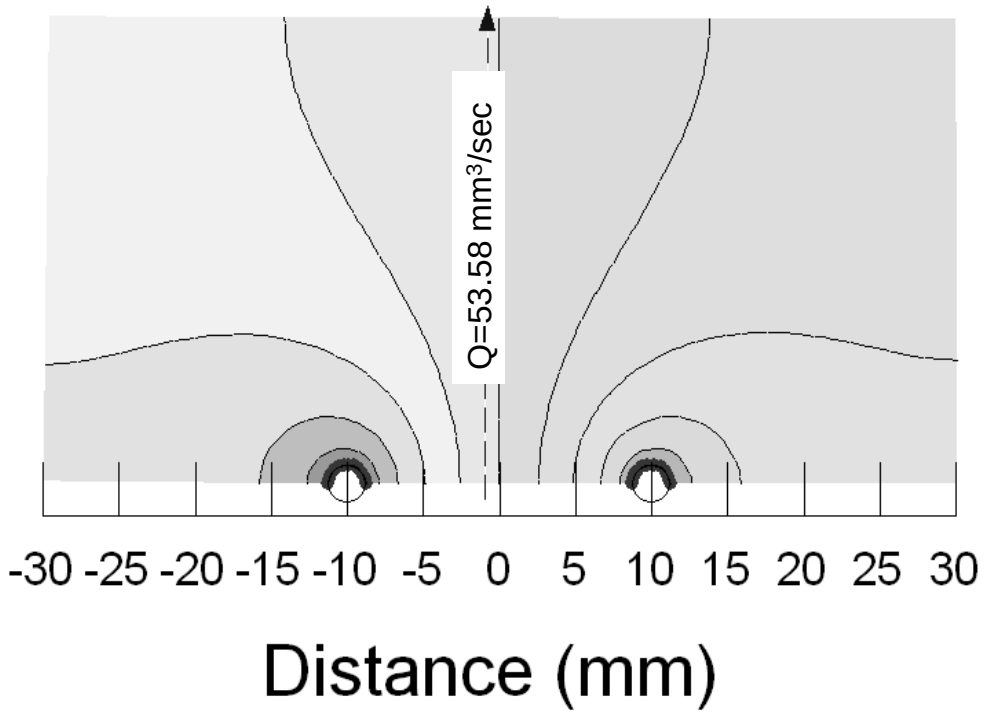

Figure 2-11 Equipotential contours, each representing 10 millimeters of hydraulic head loss (10 Volts of potential loss), for two 2.5 millimeter diameter rods spaced 20 millimeters apart

The three rod probe consists of three 0.48 centimeter diameter rods spaced 4.5 centimeters apart. The center rod was assigned a hydraulic head of 100 centimeters (100 Volts) and the outer rods were assigned a hydraulic head of 0 centimeters (0 Volts). Contour plots of the resulting equipotential representing 10 inches of head loss (10 Volts of potential loss) were created and the flow rate through the section was reported (Figure 2-12).

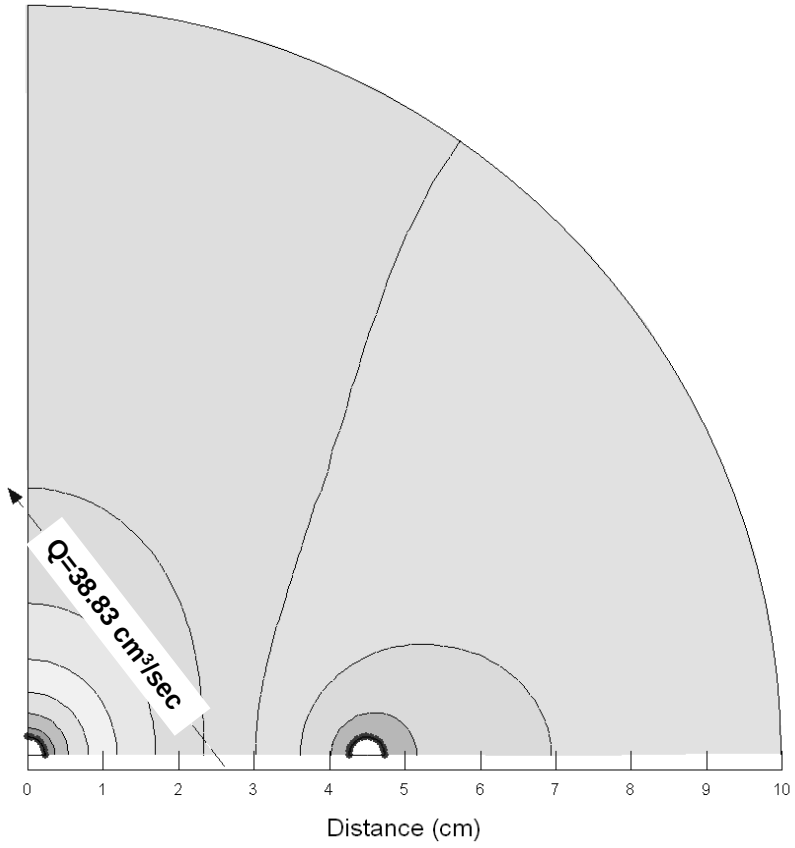

Figure 2-12 Equipotential contours, each representing 10 centimeters of hydraulic head loss (10 Volts of potential loss), for three 0.48 centimeter diameter rods spaced 4.5 centimeters apart

The two rod probe configuration shows that the energy loss is symmetric with respect to a center axis between the two rods which is consistent with the electromagnetic field for the same two rod probe reported by Becker et al., (2006). The three rod configuration also shows symmetry about a center axis, however, similar to the coaxial probe configurations a majority of the energy is concentrated around the center rod. This observation is consistent with those made by Robinson et al., (2003). Because these configurations do not represent coaxial conditions equation 2.2 does not apply. Robinson et al. (2003) defines a geometric factor for a two rod probe as:

$$g = \frac{12.1 \cdot L}{\ln\left[\frac{s}{d} + \sqrt{\left(\frac{s}{d}\right)^2 - 1}\right]} \qquad \text{Eq. 2.10}$$

where L is the length of the probe, s is the spacing between the rods, and d is the rod diameter. Based on this relationship and the same assumptions used to derive equation 2.5, the shape factor for two rod probe configurations can be defined by:

$$\frac{n_f}{n_d} = \frac{12.1}{\ln\left[\frac{s}{d} + \sqrt{\left(\frac{s}{d}\right)^2 - 1}\right]} \qquad \text{Eq. 2.11}$$

Inserting the rod spacing and diameter into equation 2.11, the shape factor is computed as 4.37; however, Robinson et al. (2003) recommend that equation 2.10 not be used for measurement because it is only an approximation. The shape factor obtained from the flow rate reported by the model is 1.07, which is significantly lower. The shape factor for the three rod probe obtained from the flow rate is 1.55. The geometric factor used for two and three rod probes are typically found through calibrations which produce more reliable values. This modeling provides relatively accurate geometric factors for coaxial configurations, but it is unclear how well the method works for two and three rod probe configurations.

2.5. Results and Recommendations

The finite difference and finite element methods were used to evaluate different TDR probe geometries in an effort to increase the accuracy and continuity of electrical conductivity measurements in soils both in the laboratory and in the field. Table 2-1 presents the flow rates obtained for each configuration. These flow rates were used to calculate the shape factors using equation 2.9. These factors as well as those obtained using the finite difference method are reported in Table 2-2.

Table 2-1 Flow rates obtained by the finite element method using SEEP/W

Configuration	Wedge Flow Rate (in^3/s)	Overall Flow Rate (in^3/s)
5/16" Center Spike 4" Cylinder	40.84	245.0
3/8" Center Spike 6" Cylinder	37.78	226.7
3/8" Spikes 2.588" Spacing w/ Zero Boundary	36.49	218.9
3/8" Spikes 2.588" Spacing Semi-Infinite Boundary	33.65	201.9
4-3/8" Spikes 2.588" Spacing inside 6" Cylinder	38.74	232.4
4-3/8" Spikes 2.588" Spacing inside 11" Cylinder	35.75	214.5

Table 2-2 Calculated shape factors

		Finite Difference Method	Finite Element Method
5/16" Center Spike 4" Cylinder	60° Wedge	0.425	0.408
	Overall	2.55	2.45
3/8" Center Spike 6" Cylinder	60° Wedge	0.423	0.378
	Overall	2.54	2.27
3/8" Spikes 2.588" Spacing w/ Zero Boundary	60° Wedge	0.37	0.365
	Overall	2.22	2.19
3/8" Spikes 2.588" Spacing Semi-Infinite Boundary	60° Wedge	n/a	0.336
	Overall	n/a	2.02
3/8" Spikes 2.588" Spacing inside 6" cylinder	60° Wedge	n/a	0.387
	Overall	n/a	2.32
3/8" Spikes 2.588" Spacing inside 11" cylinder	60° Wedge	n/a	0.357
	Overall	n/a	2.14
3-0.48 cm Spikes 4.5 cm spacing, semi-infinite boundary	90° Wedge	n/a	0.388
	Overall	n/a	1.55
2-2.5 mm Spikes 20 mm spacing, semi-infinite boundary	180° Wedge	n/a	0.536
	Overall	n/a	1.07

To confirm the validity of the calculated shape factors, the dimensions of the two coaxial configurations were entered into equation 2.5. The theoretical shape factors for the 5/16 inch diameter center spike inside of a 4 inch diameter cylinder and for the 3/8 inch diameter center spike inside of a 6 cylinder are 2.465 and 2.266, respectively. These factors are similar to those obtained using the finite element method, 2.45 and 2.27, respectively, but are much lower than those obtained using the finite difference method.

The finite difference method can be used as an approximation; however, the manual aspect of calculating the number of flow channels can introduce significant errors in the results. The finite element method is proven to provide more accurate and consistent results. With the advancement of computer technology the current software programs are simple to use and models are easy to modify. Although it can be a mistake to assume that the software outputs are correct. The results depend on the user inputs and clear understanding of the processes involved is required to properly utilize the capabilities of the program. It is advantageous to use another method such as the finite difference or hand drawn flow nets to estimate an answer before running the models to ensure reasonable results.

The computer software also allowed further investigation of the effects of introducing a zero head boundary to the four rod field probe configuration. Figure 2-7 and Figure 2-8 illustrate the effects on the equipotential contours and the head loss behavior of the system. In the case where the zero head boundary is imposed the head loss occurs faster and the flow rate is higher. By introducing the boundary, there is a finite distance at which the head must be equal to zero in addition to the outer spikes. In reality the head is only zero at the outer spikes and residual energy slowly dissipates as it moves towards an infinite distance from the source. This slow dissipation of energy reduces the flow rate between the inner and outer spikes resulting in a smaller shape factor.

The shape factors are different for each of the probe configurations investigated, which implies that a different value of the constant *C'* should be used for different probe geometries. Current TDR software programs calculate *C'* based on the ratio of the outer conductor diameter to the inner conductor diameter (*R/r*). The ratio can by obtained by solving equation 2.5 for *R/r*:

$$\frac{R}{r} = \exp(2\pi /(n_f / n_d)) \qquad \text{Eq. 2.12}$$

Table 2-3 is a summary of the equivalent ratios corresponding to each of the probe geometries: also provided is a correction factor for electrical conductivity values obtained using the previously assumed value of 12.9 for all probe configurations. Although the two and three rod probes are not coaxial configurations, the software program require and equivalent R/r ratio to obtain the electrical conductivity. Therefore, using the shape factors obtained for the two and three rod probes and equivalent R/r can be found using equation 2.10; however, these values are only approximate and may not truly represent the electromagnetic conditions.

Table 2-3 Equivalent outer to inner conductor diameter ratios and conductivity corrections

Configuration	Overall Flow Rate (in^3/s)	n_f/n_d	R/r or Equivalent R/r	Conductivity Multiplier
PMTDR and MDI-PDA values for all tests	NA	2.46	12.9*	1
5/16" Center Spike 4" Cylinder	245.0	2.45	12.8	1.004
3/8" Center Spike 6" Cylinder	226.7	2.27	16.0	1.084
4-3/8" Spikes 2.588" Spacing inside 6" Cylinder	232.4	2.32	15.0	1.060
4-3/8" Spikes 2.588" Spacing inside 11" Cylinder	214.5	2.14	18.8	1.150
4-3/8” Spikes 2.588” Spacing with semi-infinite boundary	201.9	2.02	22.5	1.218
3-0.48 cm Spikes 4.5 cm spacing, semi-infinite boundary	155.32	1.55	57.6	1.585
2-2.5 mm Spikes 20 mm spacing, semi-infinite boundary	107.16	1.07	355	2.296

* Value assumed in PMTDR, MDI-PDA, and MDI-PC software.

This investigation effectively shows that the geometry of the probe can significantly affect the TDR-measured electrical conductivity. It is important to model new geometric configurations to ensure accurate measurements in both the field and in the laboratory.

CHAPTER 3. TEMPERATURE EFFECTS ON THE APPARENT DIELECTRIC CONSTANT DETERMINED BY TIME DOMAIN REFLECTOMETRY

3.1. Introduction

Time domain reflectometry (TDR) is a widely used technique for measuring the water content of soils. The dielectric properties of a soil can be determined by measuring the propagation velocity of electromagnetic waves traveling through the medium. The composite dielectric constant is a combination of the individual dielectric constants of the soil components (solid soil particles, air and water). The apparent dielectric constant of water ($K_{a,water} \approx 80$) is significantly larger than the apparent dielectric constants of air and solid soil particles ($K_{a,air} = 1$, $K_{a,solids} \approx$ 2-5). Therefore changes in the measured dielectric constant for soils largely reflect changes in the amount of water (Pepin et al., 1995).

Accurate measurement of the apparent dielectric constant, K_a is critical for the estimation of the soil water content. There are many factors that could affect the measurement of K_a such as porosity, soil specific surface area, geometric arrangement of particles and temperature (Robinson et al., 2006, Wraith and Or, 1999), but this chapter will mainly focus on the effects of temperature. This study uses TDR data collected for a variety of soils at temperatures ranging from 4°C to 40°C to identify temperature correction factors, if necessary, for the measurement of apparent dielectric constant in soils.

3.2. Background Information

The accurate measurement of the apparent dielectric constant (K_a) is an integral part of the measurement of water content using Time Domain Reflectometry (TDR). The most often used relationship between the apparent dielectric constant and volumetric

water content is Topp's Equation (Topp et al., 1980) which reflects an increase in K_a with increasing volumetric water content. Nonetheless, there are many factors that can influence the measurement of the dielectric properties of soils including porosity, soil specific surface area, geometric arrangement of the soil particles and temperature (Robinson et al., 2006, Wraith and Or, 1999). It also has been reported that the electrical conductivity of the soil can affect the measured values of the apparent dielectric constant (Benson and Wang, 2006).

Temperature effects on the apparent dielectric constant measured by TDR have been previously identified (Pepin et al., 1995; Or and Wraith, 1999; Drnevich et al., 2001) and while the effects on the apparent dielectric constant of water are well understood (Weast, 1986), the effects on the apparent dielectric constant of soils are still being investigated. These earlier studies covered a broad range of conditions and soil types. Volumetric water contents varied between 0 and 0.81, temperatures range from -22 to 65°C. Both coarse and fine grained soils including peats have been investigated in these studies.

Some studies have concluded that temperature effects on the apparent dielectric constant were limited and did not have a significant effect on the resulting water content determination while others suggested that temperature could affect the apparent dielectric constant and the inferred water content. Topp et al. (1980) concluded that there was no strong temperature dependence on K_a for temperatures between 10°C to 36°C and volumetric water contents from 0 to 0.55, which was also inferred by Zagoskii et al. (1982) for temperatures above 5°C. However, below 5°C, an abrupt change in apparent dielectric constant of clay soils was observed due to a decrease in the volume of liquid water. Benson and Wang (2006) also noted that at temperatures below 0°C, K_a for silt and silty sand deceased considerably as a result of pore water freezing and ice having a lower relative dielectric constant than liquid water. For temperatures above freezing, different trends have been noted. Pepin et al. (1995) observed that the apparent dielectric constant decreased with increasing temperatures for sand, loam and saturated peat for a

range of temperatures from 5°C to 50°C. However, Or and Wraith (1999) observed that for a silt loam soil the apparent dielectric constant increased with temperature at low water content and decreased with temperature at high water content between 0°C and 65°C. Similar trends were noted by Drnevich et al. (2001), who showed that the apparent dielectric constant increased with increasing temperature for cohesive soils and decreased with increasing temperature for sands.

The common idea between the more recent studies is that the changes in the apparent dielectric constant due to temperature are related to the soil type and the moisture content of the soils. The magnitude of the change is larger for soils with high water content while those with low moisture contents exhibit smaller changes.

3.2.1. Temperature Correction Factors

Pepin et al. (1995) used a dielectric mixing model to predict the temperature effects on the TDR measurements. A mixing model proposed by Alharthi and Lange (1987) was used which relates the composite dielectric constant of a wet soil to the dielectric properties and the volume fraction of each constituent. For the soil types tested, Pepin et al. (1995) observed a decrease in apparent dielectric constant with increasing temperature except in relatively dry soils, which showed little change as a result of changing temperature. A larger difference between the predicted and measured values for soils with high water contents was also noted. A correction factor of $0.00175°C^{-1}$ for the measured volumetric water content of soil temperatures ranging between 5°C and 50°C was proposed based on the differences found between the measured and actual water content. This correction factor implies that the greater the temperature change, the greater the deviation in K_a and the resulting volumetric water content measurements. It appears that as the water content increases the influence of the temperature on K_a also increases. This explains why the temperature effects on dry soils were undetectable. The results of the study by Pepin et al. (1995) also suggested that the apparent dielectric constant of free water experiences a greater change with temperature than that of bound water. Pepin et

al. (1995) postulated that to decrease K_a in soils with significant surface-water interactions, more thermal energy needs to be introduced into the system.

A slightly different approach was used by Wraith and Or (1999) to describe the effects of temperature. They suggested that there are two competing phenomenon that affect TDR-measured values of K_a when the temperature of the system changes, which could help explain the previously presented results. The first is that the dielectric constant of the bulk water decreases as the temperature increases and the second is that there is a release of bound water in the system as the temperature increases causing the measured K_a values to increase. According to Or and Wraith (1999), these effects are governed by the soil specific surface area and water content. Together these soil characteristics determine the ratio of bound-to-bulk water present in the system which corresponds to the dominances of one process over the other. Based on these ideas they analyzed experimental data and were able to propose a correction of the apparent dielectric constant to account for temperature.

$$K_a(T+\Delta T) = K_a(T) + \frac{\partial K_a}{\partial T}\Delta T \qquad \text{Eq. 3.1}$$

The partial derivative $\partial K_a / \partial T$ is determined by relations between volume fraction of bound water content and the volume fraction of free water content. The volume fraction of bound water content is assumed to be dependent on the specific surface area of the soil and the volume fraction of free water is estimated by the sum of the bound water and the TDR-measured volumetric water content.

The Wraith and Or method involves numerous calculations which are critically based on the specific surface area of the soil. Also the estimation of one of the parameters uses the TDR-measured volumetric water content that is not corrected for temperature effects. Or and Wraith (1999) report that applying the temperature corrections to the apparent dielectric constant resulted in less ambiguous results than applying the corrections directly to the TDR-measured volumetric water content as done by Pepin et

al. (1995). Although basing some of the correction on the uncorrected measurement of volumetric water content appears contradictory; further exploration of the proposed corrections is seemingly warranted.

A third set of corrections for temperature effects was presented by Drnevich et al. (2001). This study investigated a variety of soils, both cohesive and non-cohesive, at temperatures ranging from 4°C to 40°C. For each soil at a given water content the measured apparent dielectric constant was normalized to the value measured at 20°C. The normalized apparent dielectric constant was then plotted versus temperature. It was noted that for the cohesive soils, $K_{a,normalized}$ increases with increasing temperature and decreases with increasing temperature for non-cohesive soils. It was also noted that for dry sands there was relatively little change in the apparent dielectric constant with temperature. A look at the effects of water content on cohesive soils show that at increasing water contents the temperature effects are controlled by the free water while at low water contents the soil solids and bound water dominate the behavior, which is consistent with findings from Pepin et al. (1995).

Drnevich et al. (2001) averaged values of the normalized dielectric constant at each temperature and found linear trends when plotted against temperature. They then suggest temperature corrections for the measured apparent dielectric constant using a regression line fit through the data as

$$K_{a,20^\circ C} = K_{a,T^\circ C} \times TCF \qquad \text{Eq. 3.2}$$

where *TCF* is the temperature correction function, with Eq 3.3 for cohesive soils and Eq. 3.4 for non-cohesive soils. Thus,

$$TCF = 1.10 - 0.005T_{test,T^\circ C} \text{ for cohesive soils} \qquad \text{Eq. 3.3}$$

$$\text{s}TCF = 0.97 + 0.0015T_{test,T^\circ C} \text{ for non-cohesive soils} \qquad \text{Eq. 3.4}$$

where $T_{test,T°C}$ is the temperature during the soil testing. These relationships only apply for temperatures between 4°C and 40°C. Drnevich et al. (2001) also noted that the above corrections are negligible for temperatures ranging from 15°C and 25°C.

The temperature effects on TDR-measurements are applied directly to the apparent dielectric constant by Or and Wraith (1999) and Drnevich et al. (2001) while others correct the measured volumetric water content (Pepin et al., 1995). Both approaches are valid, although if the apparent dielectric constant is used in other calculations then corrections for temperature should be applied prior to further computations.

The following investigation will analyze the effects of temperature on the TDR-measured apparent dielectric constant of both cohesive and non-cohesive soils and suggest a temperature correction to be applied directly to the measured apparent dielectric constant.

3.3. Testing Procedure

The testing for this experimental study was performed previously and reported by Drnevich et al. (2001). The TDR data were originally collected using a Tektronix 1502B Cable Tester and the resulting electromagnetic waveforms were analyzed manually. The data were later converted into a numerical file format that could be analyzed using the PMTDR-SM software. The PMTDR-SM software systematically analyzes the data to obtain the values for the apparent dielectric constant and electrical conductivity of the soil. A brief description of the actual testing procedures is presented here and a more detailed explanation can be found in Drnevich et al. (2001).

3.3.1. Soils Tested

Tests were performed on five different soils, two cohesionless and three cohesive. The properties of these soils are shown in Table 3-1. Crosby Till is a low to medium plasticity silty-clay found in the vicinity of the Purdue University campus near West Lafayette, Indiana. The Kaolinite and Illite were pure clay minerals. The concrete sand

was washed to remove the fines and the fine Ottawa sand is that commonly used in concrete research.

Table 3-1 Characteristics of soils tested

Soil	Unified Soil Classification	Atterberg Limits		Composition		
		Liquid Limit	Plastic Limit	%sand	%silt	%clay
Crosby Till	CL	41	18	16	50	34
Kaolinite	CL-ML	30	24	0	0	100
Illite	CL-CH	50	22	0	0	100
Concrete Sand	SW	NA	NA	100	0	0
Fine Sand	SP	NA	NA	100	0	0

3.3.2. Test Specimens

Specimens were prepared with a variety of water contents in a Standard Compaction Mold (ASTM D698) with a diameter of 101.6 mm (4.0 in), a height of 116.4 mm (4.584 in.) and a corresponding volume of 9.19×10^5 mm^3 (1/30 ft^3). The soil specimens were all compacted using a standard compaction of 600 kN-m/m^3 (12,400 ft-lb/ft^3).

After compaction a non-metallic guide template was temporarily placed on top of the mold and a 7.94 mm (5/16 in.) stainless steel rod was driven into the center of the specimen. The guide was removed and replaced with a metallic adapter ring, which presented a surface to support the outer three legs of the Multiple Rod Probe Head (MRPH). The center of the MRPH rested on the center rod driven into the soil. TDR measurements were made by connecting the MRPH to a Tektronix 1502B Cable Tester with a 1 m (3 ft.) coaxial cable with BNC connectors on each end.

Most specimens were tested at five different temperatures, 4°C, 10°C, 20°C, 30°C and 40°C. All specimens were prepared at room temperature, 20°C, and then placed in either an environmental test chamber or a drying oven to cool or heat the specimen to the desired target temperature. TDR measurements were recorded as a function of time to determine when the soil would equilibrate to the target temperature. It was determined that it took an average of 8 hours for the values of apparent dielectric constant and electrical conductivity to stabilize with time for a given temperature.

3.4. Evaluation of the Apparent Dielectric Constant

The TDR-measured apparent dielectric constant is used to calculate the water content of soils. It is therefore important to accurately determine the apparent dielectric constant from the TDR waveform. The TDR system estimates K_a by measuring the travel time of an electromagnetic wave propagating through the soil (Topp et al. 1980). The apparent dielectric constant is related to the velocity of the electromagnetic wave traveling through the transmission line (v) by:

$$v = \frac{c}{\sqrt{K_a}} \qquad \text{Eq. 3.5}$$

where c is the velocity of light in a vacuum.

As the wave travels through the system, two reflections occur which cause discontinuities in the TDR waveform. The first reflection occurs when the wave reaches the soil surface and the second reflection occurs when the wave reaches the end of the rods in the soil. The time difference between these points is equivalent to the time (t) required by the signal to travel twice the length of the rods in the soil (L_p). The wave propagation velocity is thus defined by:

$$v = \frac{2L_p}{t} \qquad \text{Eq. 3.6}$$

By substitution and rearranging equations 3.5 and 3.6, K_a is:

$$K_a = \left(\frac{ct}{2L_p} \right)^2 \qquad \text{Eq. 3.7}$$

To obtain the apparent dielectric constant directly from the waveform, an apparent length (L_a) equivalent to $ct/2$ is defined. L_a is the scaled distance between two points on the waveform (Figure 3-1). The first point is located at the peak of the initial reflection of the wave where the wave reaches the soil surface. The second point is the beginning of the second positive reflection, occurring when the wave reaches the ends of the probe. L_a is then related to K_a by:

$$K_a = \left(\frac{L_a}{L_p} \right)^2 \qquad \text{Eq. 3.8}$$

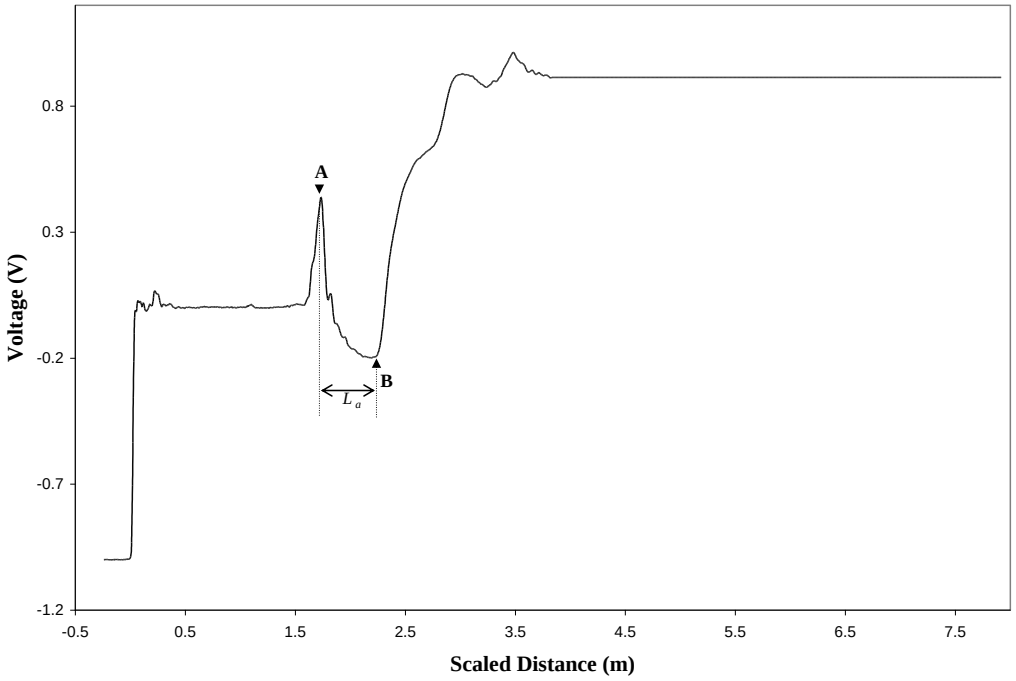

Figure 3-1 TDR waveform for fine sand, water content = 20%, point A corresponds to the peak of the first reflection where the wave reaches the soil surface, point B corresponds to the beginning of the second reflection where the wave reaches the end of the probe, and L_a is the apparent length of the waveform

3.4.1. Locating the Reflection Points from the TDR Waveform

The apparent dielectric constant is calculated based on the apparent length between two reflection points. The location of these points directly affects the calculated apparent dielectric constant; therefore, they must be identified consistently and accurately. There are three commonly used approaches to locating the reflection points from the recorded signal trace: manual analysis, computer aided analysis, and inversion analysis (Timlin and Pechepsky, 1996). The data for this investigation was previously analyzed using the manual method proposed by Baker and Allmaras (1990). This approach requires drawing tangent lines from critical sections of the TDR waveform to locate the reflection points. The results are typically satisfactory but rely heavily on the experience and judgment of the person performing the analysis. A more robust and consistent analysis method is desired.

As a solution to this problem, Yu (2003) developed the PMTDR software program for use with the Purdue TDR equipment. The algorithm is based on noise reduction and curve fittings in characteristic sections of the waveform. Details on the development of the software can be found in Yu (2003). This research utilized the PMTDR software for analysis of the apparent dielectric constant of the soils.

3.4.2. Test Results

A disadvantage to using the PMTDR software is that the algorithm is sometimes unable to locate the second reflection point leading to implausible values for the apparent dielectric constant. Values for the apparent dielectric constant of soils are a combination of the individual parts of the material (air, solids, and water). The measured Ka is expected to be greater than $K_{a,air}$ (1) and less than $K_{a,water}$ ($\approx$ 80), therefore any value not falling within this range is disregarded. Most of the recorded values are the average of at least three different tests for a given temperature and water content; however, some of the data files were either not converted to the new file format or were lost resulting in fewer data points for analysis. Table 3-2 presents the measured values of the apparent dielectric constant using the PMTDR software program.

Table 3-2 Apparent dielectric constant calculated using PMTDR software

Soil	Target Water Content (%)	Temperature (°C)				
		4	10	20	30	40
Crosby Till	3	4.22	4.34	4.45	4.44	4.51
	12	10.68	12.37	10.97	17.74	20.35
	15	16.40	16.27	16.25	19.18	20.67
	18	18.78	19.37	20.01	21.00	21.26
	21	20.95	21.38	20.84	21.29	22.13
	24	21.82	22.36	21.43	22.66	21.77
	41	29.04		28.94		34.11
Illite	20	21.77		28.33	179.90	199.96
	50	33.49		41.09	33.98	72.96
Kaolinite	20	19.98		20.90	21.00	20.57
	30	24.59		24.70		175.00
	40	31.38		30.63	33.46	35.21
Concrete Sand	dry	0.57		0.61		0.73
	saturated	18.31		17.79		16.23
Fine Sand	dry	17.90		0.08		3.23
	saturated	21.35		20.83		19.46

3.5. Effects of Temperature on the Apparent Dielectric Constant

The same soil data was previously analyzed using manual methods for effects of temperature on the TDR-measured apparent dielectric constant. As discussed previously, Drnevich et al. (2001) concluded that the apparent dielectric constant decreased with increasing temperature in cohesionless soils and increased with increasing temperature in cohesive soils.

3.5.1. Effects of Temperature on the TDR Waveforms

The apparent dielectric constant is determined by locating reflection points directly from the TDR waveform. Typically cohesive soils have a much flatter second reflection than non-cohesive soils. The second reflection tends to flatten even more when

the temperature of the soil increases. Traces of the waveforms for a given soil at the same water content show distinct changes in the location of the second reflection point as the temperature changes (Figure 3-2 and Figure 3-3).

Wraith and Or (1999) observed that the shape of the second reflection of the waveform is not only affected by temperature, but also the specific surface area of the soil. The results presented here are consistent with this observation. Waveforms of fine sand, with a relatively low specific surface area, show very little change in the shape of the second reflection (Figure 3-2). Crosby till, with a higher specific surface area, exhibits a stretching of the second reflection creating a flatter waveform (Figure 3-3). Kaolinite and Illite have the highest specific surface areas have second reflections so flat that in some cases the apparent length of the waveform cannot be determined and the apparent dielectric constant cannot be measured, (Figure 3-4).

Figure 3.2 illustrates the waveforms of cohesionless fine sand. Unlike the Crosby till, the shape of the waveform is not altered that much as the temperature changes. Wraith and Or (1999) present similar findings for a Kidman sandy loam. Also the location of the second reflection point shifts to the left as opposed to the right. This corresponds to a decrease in the apparent length and subsequently the apparent dielectric constant. This reflects a decrease in K_a as temperature increases as previously reported by Pepin et al. (1995) and Drnevich et al. (2001) for cohesionless soils. The shape of the second reflection is relatively unaffected by the temperature change in the sand implying that even large changes in temperature do not necessarily have a large impact on the apparent dielectric constant.

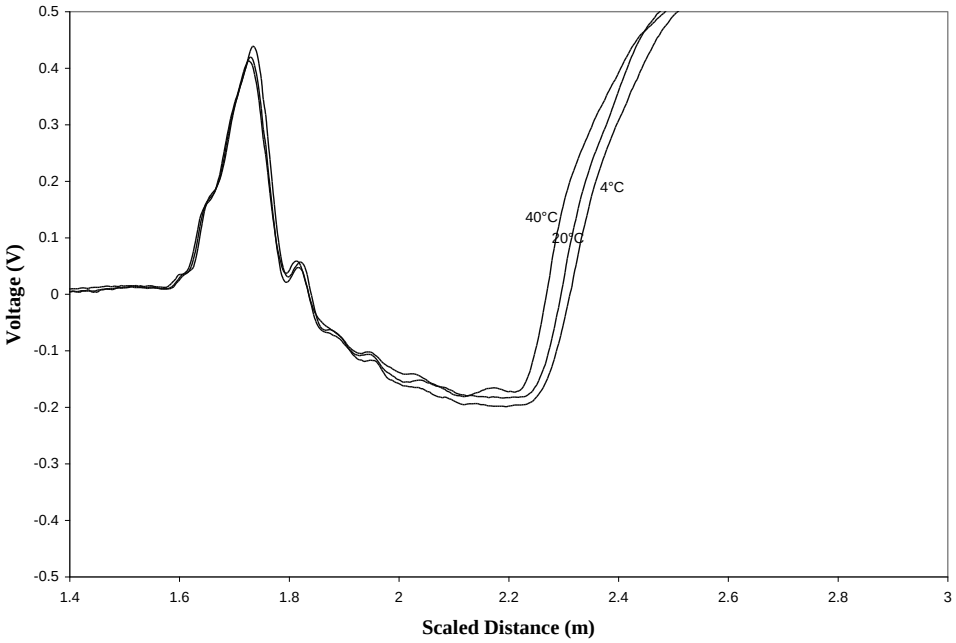

Figure 3-2 TDR waveforms for fine sand, water content = 20%, temperatures ranging from 4°C to 40°C

Crosby till is a silty-clay with low to medium plasticity and is considered relatively cohesive. At a moderate water content of 18%, the second reflection point on the TDR waveform shifts slightly to the right as the temperature increases (Figure 3-3b). The reflection also dips lower as temperature increases which could be impacted by the electrical conductivity as it changes with temperature, which will be further explored in chapter 4. This shape is consistent with the shape of TDR waveforms from Brocko silt loam reported by Wraith and Or (1999). By shifting the second reflection point to the right the apparent length of the waveform increases which corresponds to an increase in the measured apparent dielectric constant. This increase in Ka as temperature increases is in agreement with Drnevich et al. (2001) for cohesive soils. However, for Crosby till with water content of 15% the waveforms are not as consistent as temperature changes (Figure 3-3a). The second reflection for temperatures above 20°C actually overlaps the others. Some interference could be caused by the multiple reflections that occur from the probe

head that can be seen as noise in the waveform after the first reflection. It appears that this interference can cause the beginning of the second reflection point to shift leading to an overestimation of the apparent dielectric constant.

Kaolinite and Illite exhibit similar behavior as the temperature increases. Both waveforms flatten as the temperature increases. In some cases it is impossible to locate the second reflection point and the apparent dielectric constant of the soil cannot be determined. Hook and Livingston (1995) and Wraith and Or (1999) observed that these "flatter" reflections increase the uncertainty in the measured apparent dielectric constant leading to greater scatter in the measurements.

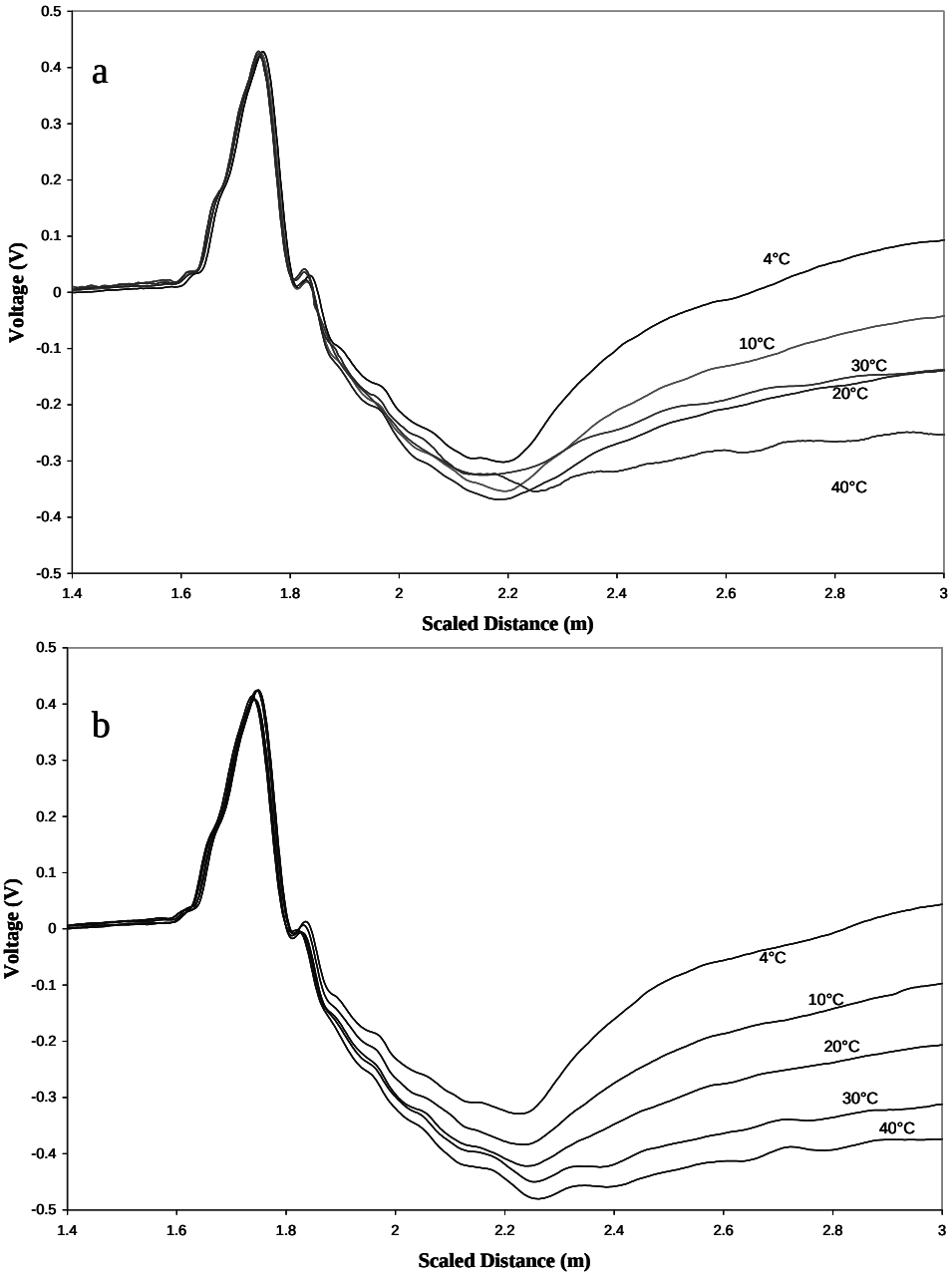

Figure 3-3 TDR waveforms for Crosby till, a) water content = 15%, b) water content = 18%, temperatures ranging from 4°C to 40°C

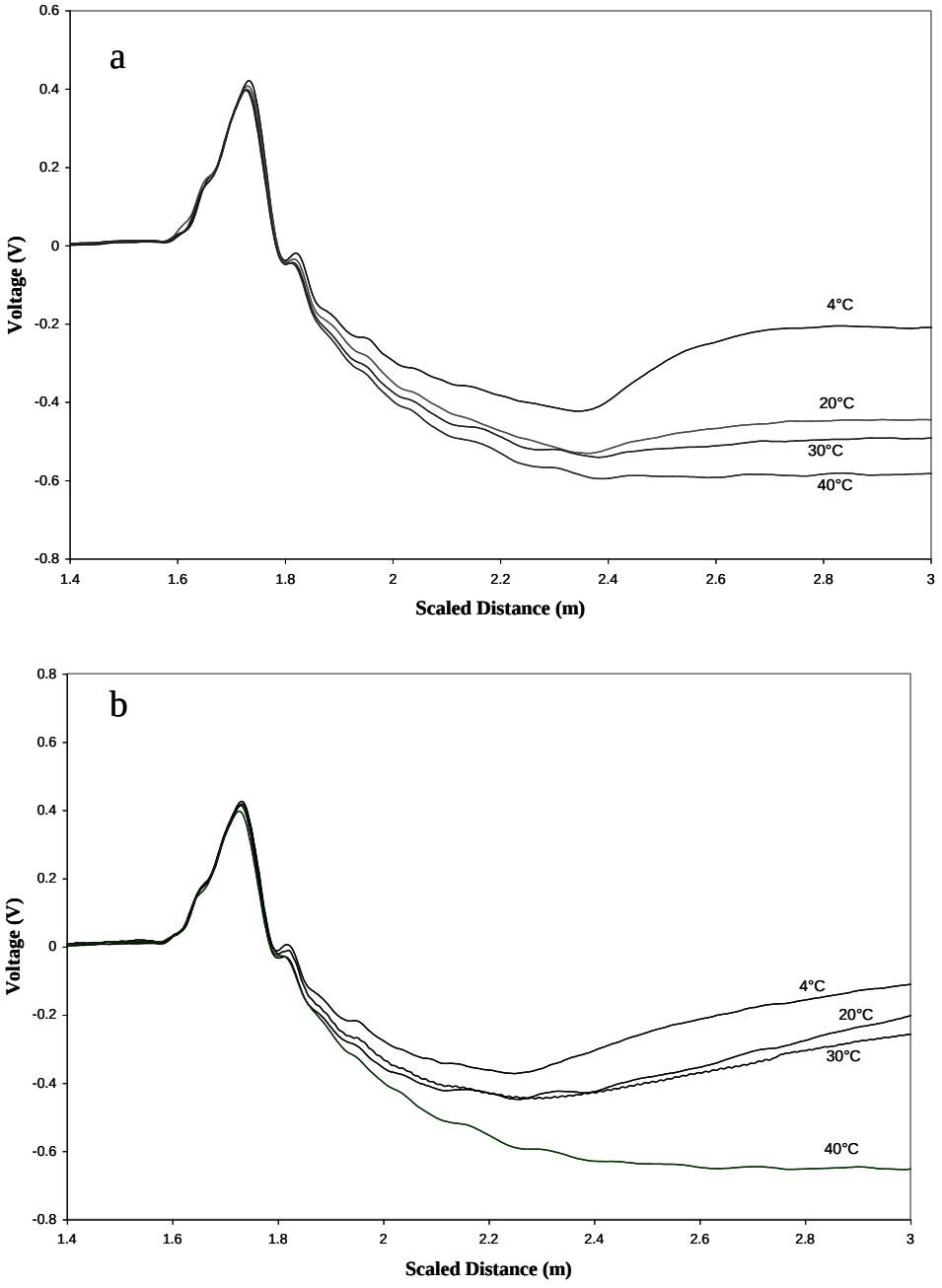

Figure 3-4 TDR waveforms for a) Kaolinite water content = 40%, b) Illite water content = 20%, temperatures ranging from 4°C to 40°C

3.5.2. Normalized Apparent Dielectric Constant

The normalized apparent dielectric constant is obtained by dividing the measured values reported in Table 3-2 by the measured apparent dielectric constant at 20°C for a given soil at the same water content. The results are plotted in Figure 3-5. Some interesting observations can be made from the chart. Crosby till with water contents of 12% and 15% do not really follow a trend and have exceptionally high normalized apparent dielectric constants for temperatures of 30°C and 40°C, especially at 12%. Also a large number of cohesive soil samples resemble cohesionless soils at temperatures less than 20°C. A possibility of the discrepancies could be that the apparent dielectric constant at 20°C is not accurate. The use of a computer algorithm and the averaging of the results could also contribute to the scatter in the data. In some soils, there is a fluctuation as the temperature increases which could be caused by a slight misinterpretation of the waveform.

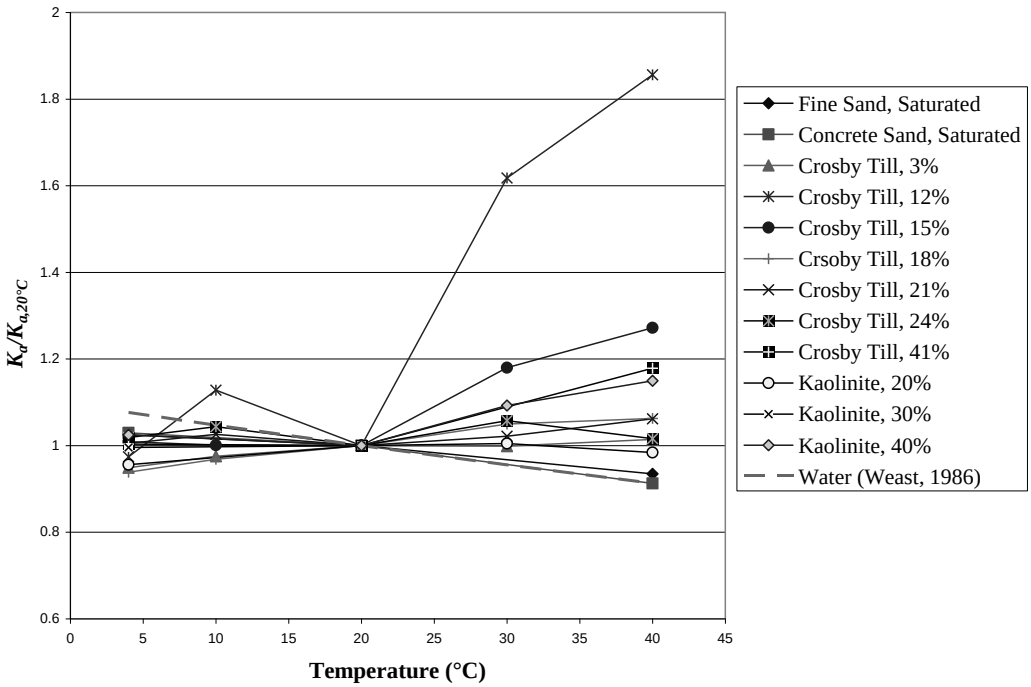

Figure 3-5 Normalized apparent dielectric constant versus temperature

There is a lot of scatter in the data and it is difficult to identify clear trends. Plots of the measured apparent dielectric constant versus temperature were made for each soil and water content. Best fit lines through the data were drawn and equations for the lines were used to calculate approximate values of the apparent dielectric constant corresponding to each temperature. These values were then normalized to 20°C and plotted in Figure 3.6. The trends associated with the change in apparent dielectric constant as the temperature increases are easily identifiable. With the exception of Crosby till, water content 12%, the normalized K_a increases with increasing temperatures within a range of approximately 0.9 to 1.15. This range is consistent with those reported by Drnevich et al. (2001). The obvious irregularity found in Crosby till, water content 12% is a result of the large variation in measured apparent dielectric constant (almost doubling) over this temperature range. It appears that the measured K_a at 20 may be the primary cause of the unusual trend noted for Crosby till, water content 12%; however, by disregarding this point and fitting a line through the remaining data points still shows a significantly larger variation with temperature than the other soils. These abnormalities cannot be fully explained without more testing of this soil. For the purposes of this study this data set is unreliable and was discarded. Analysis was preformed on the remaining soils.

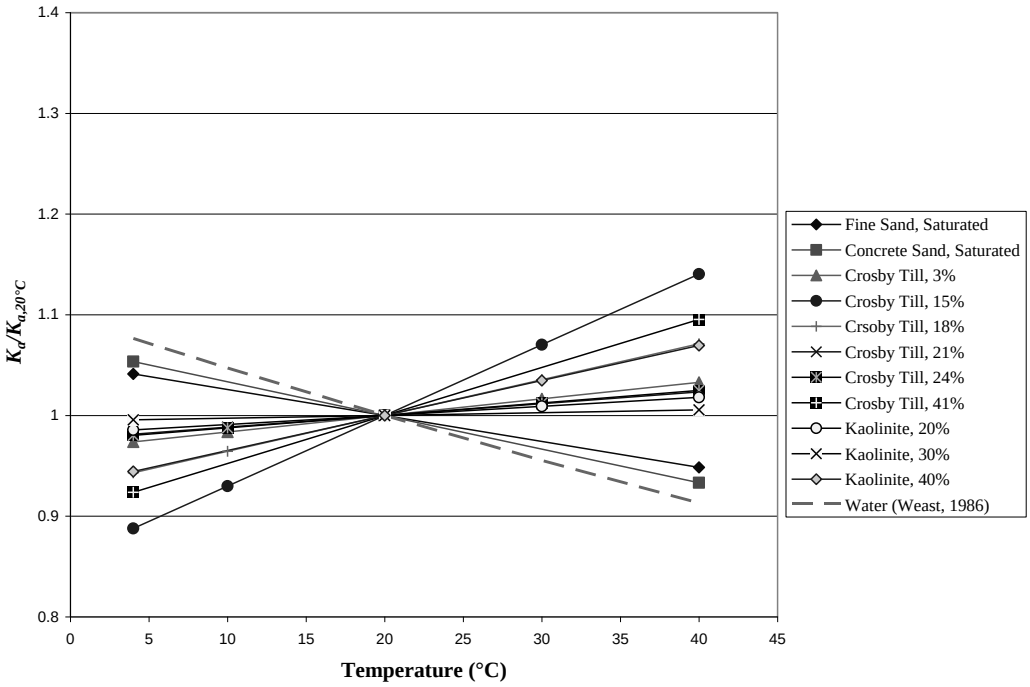

Figure 3-6 Normalized apparent dielectric constant versus temperature of calculated values based on the best fit lines for each soil and water content

3.6. Correction Recommendations

The average of the cohesive soils at each temperature is plotted in Figure 3-7. The best fit line represents the temperature correction factor that should be applied to the measured apparent dielectric constant to more accurately predict K_a at 20°C. The *TCF* (Eq. 3.3) proposed by Drnevich et al. (2001) is also illustrated on the plot. The averaged values show that the normalized apparent dielectric constant ranges between approximately 0.96 and 1.05 which is a smaller range than previously reported. The updated correction factor (Eq. 3.9) can be directly applied to the relationship defined by Equation 3.2.

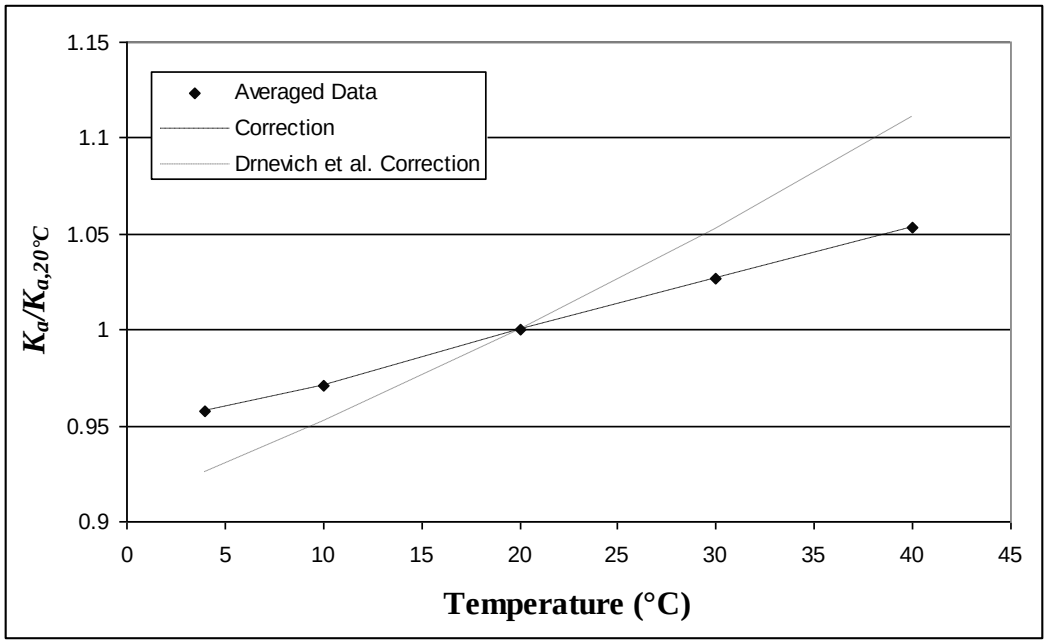

Figure 3-7 Average normalized apparent dielectric constant versus temperature with the new correction and the previous Drnevich et al. (2001) correction for cohesive soils

$$TCF = 1.054 - 0.0027 T_{test,T^{\circ}C} \quad \text{for cohesive soils} \qquad \text{Eq. 3.9}$$

Figure 3-8 shows the original data points for cohesive soils, excluding those discarded for analysis, along with the new correction factor in addition to the Drnevich et al. (2001) correction. There is a lot of scatter for the measured values of K_a at 40°C. Crosby till, water contents 15% and 41% have higher than expected values of K_a compared to the other tests. Also kaolinite, water content 20% has a value lower than expected at 40°C. Crosby till, water content 15% at a temperature of 30°C seems suspect. These irregular values are most likely the result of misidentifying the reflection points. With the exception of these points the measured values fall within approximately +/- 6% of the proposed correction and approximately +/- 9% of the Drnevich et al. (2001) correction.

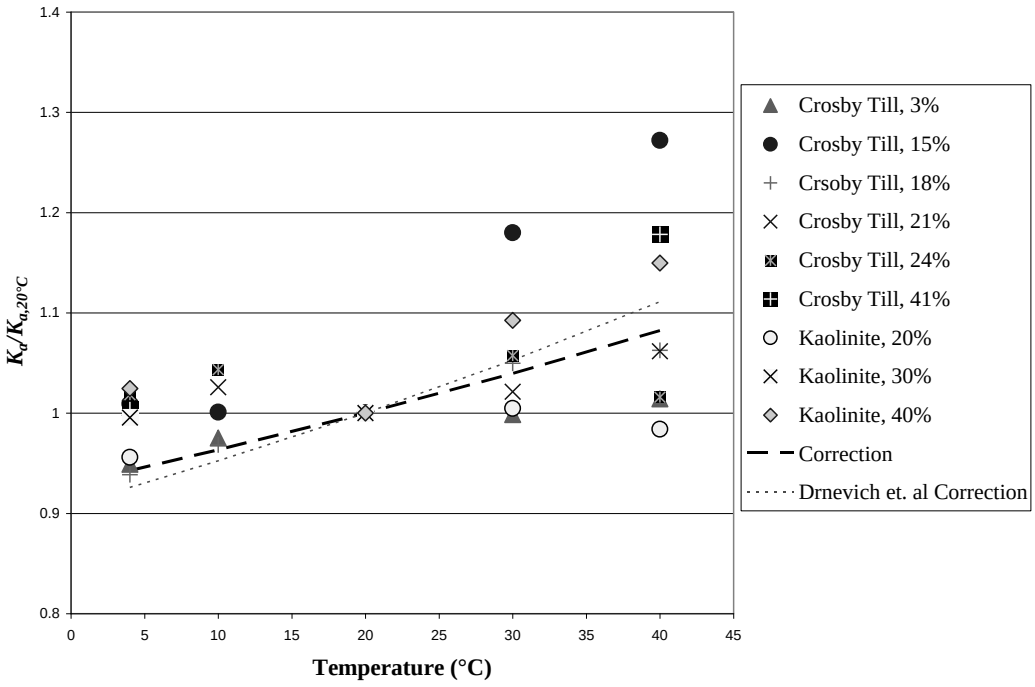

Figure 3-8 Measured values of normalized apparent dielectric constant versus temperature with the new correction and the previous Drnevich et al. (2001) correction for cohesive soils

The same analysis was also preformed on the cohesionless soils. A slightly larger range of values is noted for this analysis. This could be a factor of fewer non-cohesive samples. The apparent dielectric constant measured by PMTDR in dry sands was erroneous and therefore analysis using these samples was not possible. Figure 3-9 shows the averaged data along with the Drnevich et al. (2001) correction for non-cohesive soils. Based on the best fit line through the data the *TCF* of cohesionless soils can be defined as:

$$TCF = 0.94 + 0.003T_{test,T^{\circ}C} \quad \text{for non-cohesive soils} \qquad \text{Eq. 3.10}$$

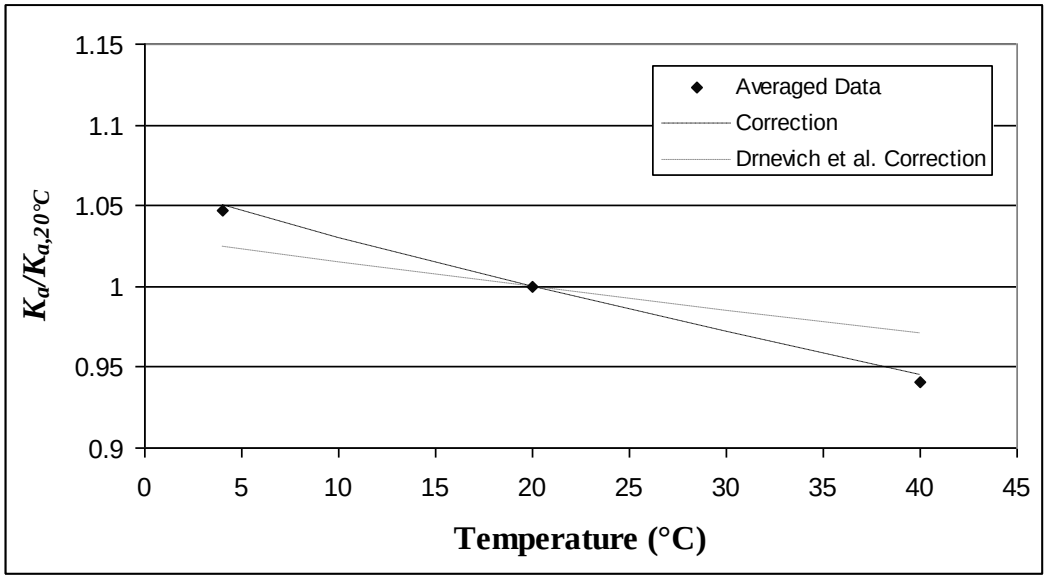

Figure 3-9 Average normalized apparent dielectric constant versus temperature with the new correction and the previous Drnevich et al. (2001) correction for non-cohesive soils

Figure 3-10 shows the original data points for non-cohesive soils along with the new correction factor in addition to the Drnevich et al. (2001) correction. The new correction fit to these data points appears to be an average between the relationship for water and the Drnevich et al. correction. The new correction slightly overestimates K_a at 40°C and underestimates K_a at 4°C. The maximum error associated with the new correction is approximately +/- 3% and the maximum error is approximately +/- 6% for the Drnevich et al. correction and water.

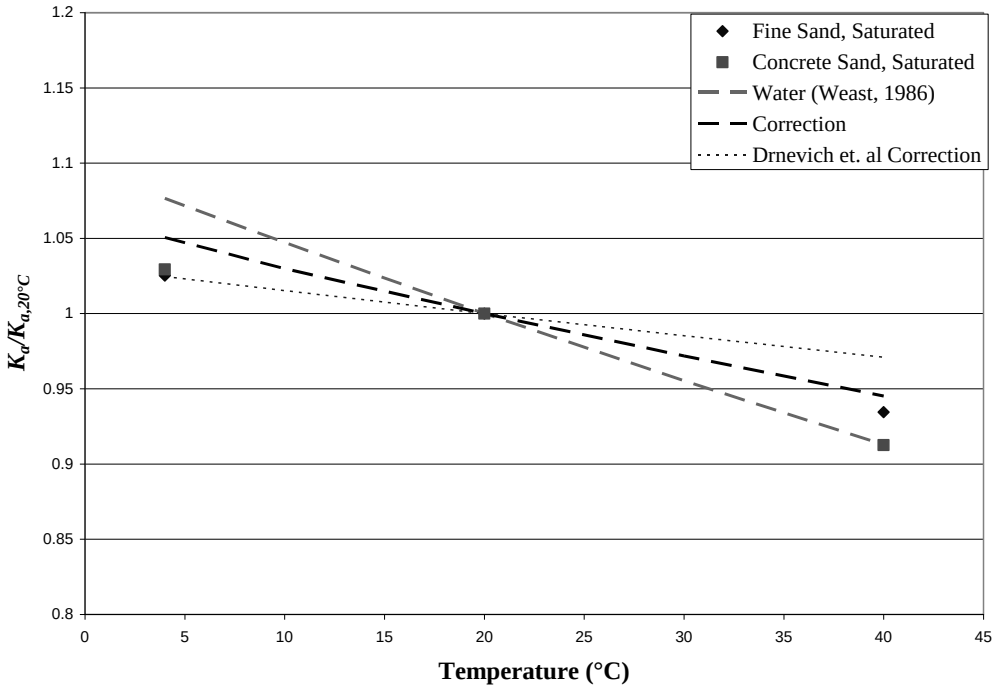

Figure 3-10 Measured values of normalized apparent dielectric constant versus temperature with the new correction and the previous Drnevich et al. (2001) correction for non-cohesive soils

Either the Drnevich et al. (2001) or the new proposed linear temperature correction factors can be applied to the apparent dielectric constant measured at any temperature to normalize to the value at 20°C. The gravimetric water content and dry density is related to the apparent dielectric constant through the calibration equation (3.11) developed by Siddiqui and Drnevich (1995).

$$\sqrt{K_a}\,\frac{\rho_w}{\rho_d} = a + bw \qquad \text{Eq. 3.11}$$

where a and b are soil-type depended constants, ρ_w is the density of water, and ρ_d is the dry density of the soil.

From equation 3.11, the water content is related to the square root of the apparent dielectric constant therefore the small effects of temperature on K_a correspond to even smaller effects on the water content.

CHAPTER 4. TEMPERATURE EFFECS ON THE ELECTRICAL CONDUCTIVITY DETERMINED BY TIME DOMAIN REFLECTOMETRY

4.1. Introduction

The d.c. electrical conductivity (EC_b) also can be measured using Time Domain Reflectometry (TDR). The electrical conductivity measurement combined with the apparent dielectric constant measurement can be used to determine the soil water content and dry density using a single TDR test (Yu and Drnevich, 2004). Corrections for temperature effects are critical for accurate determination of these two soil characteristics.

The electrical conductivity of soils can be linked to the electrical conductivity of pore water (Heimovaara et al., 1995; Persson and Berndtsson, 1998; Wraith and Or, 1999). The effect of temperature on EC_b of soil is then expected to follow the same trends as EC_b of water. This study uses TDR-collected data for a variety of soils at temperatures ranging from 4°C and 40°C to identify temperature corrections for the measured electrical conductivity of soils.

4.2. Background Information

The electrical conductivity of water has been thoroughly characterized (Stogryn (1971); Ulaby et al. (1986); Robinson and Stokes, 1959; Franson, 1985). Studies have also been performed using similar relationships to examine the temperature effects on the electrical conductivity of soils (Heimovaara et al., 1995; Persson and Berndtsson, 1998; Wraith and Or, 1999). Unlike the effects of temperature on the apparent dielectric constant, there is agreement between studies showing that the measured electrical conductivity increases as temperature increases and is relatively independent of soil type,

specific surface area or other soil properties. Heimovaara et al. (1995) identified three factors that control the electrical conductivity of the soil. The first factor is the electrical conductivity of the solution present in the soil, in most instances this is water. The second factor is the effective volumetric water content which is the available volume of water through which the electrical current can flow. The remaining portion of the volumetric water content is hindered by its closeness to the soil particles, also referred to as the bound water. The third factor accounts for the influence of the tortuosity of the ion flow lines in the soil on the mobility of the ions.

Wraith and Or (1999) briefly discuss the effects of temperature on the measured electrical conductivity for temperatures ranging between 0°C and 65°C. They found that the correction equation (Eq. 4.1) for aqueous solutions proposed by Stogryn (1971) and Ulaby et al. (1986) could be used to reasonably predict the response of the soil bulk electrical conductivity measured in their experiments until the temperature reached 40°C. At 40°C, the relationship fails and grossly underestimates the measured electrical conductivity at this temperature. A possible explanation is provided by Sen and Good (1992) who propose that as temperature increases, the electrical conductivity of the water increases and the mobility of counter-ions also increases resulting in a much larger measurement of EC_b in soils at high temperatures. This phenomenon is linked to the tortuosity of the ion flow lines affecting the electrical conductivity mentioned by Heimovaara et al. (1995).

$$EC_{water}(T) = EC_{water,25^{\circ}C} \exp\left\{\Delta'(2.033\times10^{-2} + 1.266\times10^{-4}\Delta' + 2.464\times10^{-6}\Delta'^{2})\right\} \quad \text{Eq. 4.1}$$

where Δ' is (25-T) °C and $EC_{water,25°C}$ is in dS/m.

Heimovaara et al. (1995) addressed the effects of temperature on EC_b for temperature ranging from 0°C to 30°C. First, they introduce an equation (Eq. 4.2) which defines the electrical conductivity at a standard temperature of 25°C.

$$EC_{b,25} = (K_p / R_s) f_T \quad \text{Eq. 4.2}$$

where K_p is the cell constant of the probe (m^{-1}) (Heimovaara et al. (1995) used a triple wire probe), R_s is the electrical resistance of the sample (Ω) and f_T is the temperature factor. The temperature factor is described by (Franson, 1985):

$$f_T = 1/[1+\alpha(T-25)] \qquad \text{Eq. 4.3}$$

where α is a temperature coefficient related to the sample.

The temperature coefficient reported by Heimovaara et al. (1995) of $0.019°C^{-1}$ was calculated using a least squares optimization. This value is almost identical to the temperature coefficient of $0.02°C^{-1}$ near 25°C for aqueous solutions presented by Robinson and Stokes (1959). This shows that the temperature dependence of the bulk soil electrical conductivity is apparently the same as the temperature dependency of the electrical conductivity of the aqueous solution present in the soil. Persson and Berndtsson (1998) obtained a temperature coefficient of $0.0191°C^{-1}$ to correct electrical conductivity for changes in temperature. Persson and Berndtsson (1998) concluded that unlike the effect of temperature on the apparent dielectric constant, the effects on the electrical conductivity are relatively independent of soil texture.

The following investigation will analyze the effects of temperature on the TDR-measured electrical conductivity of both cohesive and non-cohesive soils and suggest a temperature correction to be applied directly to the measured electrical conductivity.

4.3. Testing Procedures

The electrical conductivity of a variety of soils was measured using time domain reflectometry. The specifics of the testing process and soil type information has been previously discussed in section 3.3.

4.4. Evaluation of the Electrical Conductivity

The electrical conductivity is calculated using equation 2.1 as previously discussed in section 2.2. The source voltage, V_s, is the difference between the average

voltage of approximately 25 points before the reflection caused by the probe head and the voltage of approximately the first 25 points at the start of the signal. The final voltage, V_f, is the difference between the average voltage of approximately the last 25 points and the first 25 points at the start of the signal. TDR measurements were made using a 5/16 inch center spike inside of a 4 inch-diameter cylinder; therefore, *C'* (Eq. 2.2) was calculated using a ratio of outer conductor diameter to inner conductor diameter equal to 12.8 (Table 2-3).

4.4.1. Test Results

The PMTDR program most often produces reliable measurements of the electrical conductivity. The determination of the source and final voltages is much simpler than locating the second reflection point needed to compute the apparent dielectric constant of the soil. Most of the recorded values are the average of at least three different tests for a given temperature and water content; however, some of the data files were lost resulting in fewer points for analysis. Table 4-1 presents the measured values of the electrical conductivity reported in units of milliSiemens per meter (mS/m).

Table 4-1 Electrical conductivity (mS/m) calculated using PMTDR software

Soil	Target Water Content (%)	Temperature (°C)				
		4	10	20	30	40
Crosby Till	3	1.28	1.92	1.85	2.43	2.74
	12	31.97	48.61	57.65	77.21	89.75
	15	44.55	61.02	75.54	84.47	146.85
	18	48.11	67.11	86.67	116.18	135.83
	21	48.47	62.25	77.17	107.59	59.19
	24	42.41	62.62	72.62	80.81	127.78
	41	43.22		78.25		125.74
Illite	20	55.40		202.15	293.67	338.37
	50	189.61		307.62	120.49	20.13
Kaolinite	20	88.42		98.44	126.77	39.44
	30	101.13		170.91		236.45
	40	100.07		177.35	203.88	268.40
Concrete Sand	dry	0.39		0.38		-0.22
	saturated	3.16		5.20		7.72
Fine Sand	dry	0.91		0.93		0.93
	saturated	3.16		3.45		7.00

4.5. Effects of Temperature on the Electrical Conductivity

The soil data was previously analyzed for the effects of temperature on the apparent dielectric constant but not for the effects of temperature on the electrical conductivity. Other studies of the electrical conductivity have concluded that the temperature behavior emulates the effects of temperature on the electrical conductivity of water which increases as the temperature increases (Heimovaara et al., 1995).

4.5.1. Effect of Temperature on the TDR Waveforms

The electrical conductivity is determined from the waveform by measuring the source voltage and the final voltage. High electrical conductivities occur when the final voltage is much smaller than the source voltage (Eq. 2.1). The second reflection of the

TDR waveform is not as distinguishable in cohesive soils as cohesionless soils. The second reflection does not experience a sharp jump in voltage which leads to smaller final voltages and to higher values of the electrical conductivity.

When dry, the waveforms of fine sand at different temperatures are the same (Figure 4-1a). This observation implies that the electrical conductivity of dry sands is not affected by changes in temperature. When saturated, it can be seen that there are some variations in the waveforms as the temperature changes. In the previous chapter it was noted that the second reflection point at higher temperatures is located to the right of the others. Near the end of the second reflection the waveforms cross so that the final voltage at warmer temperatures is lower than the colder temperatures which correspond to an increase in the electrical conductivity.

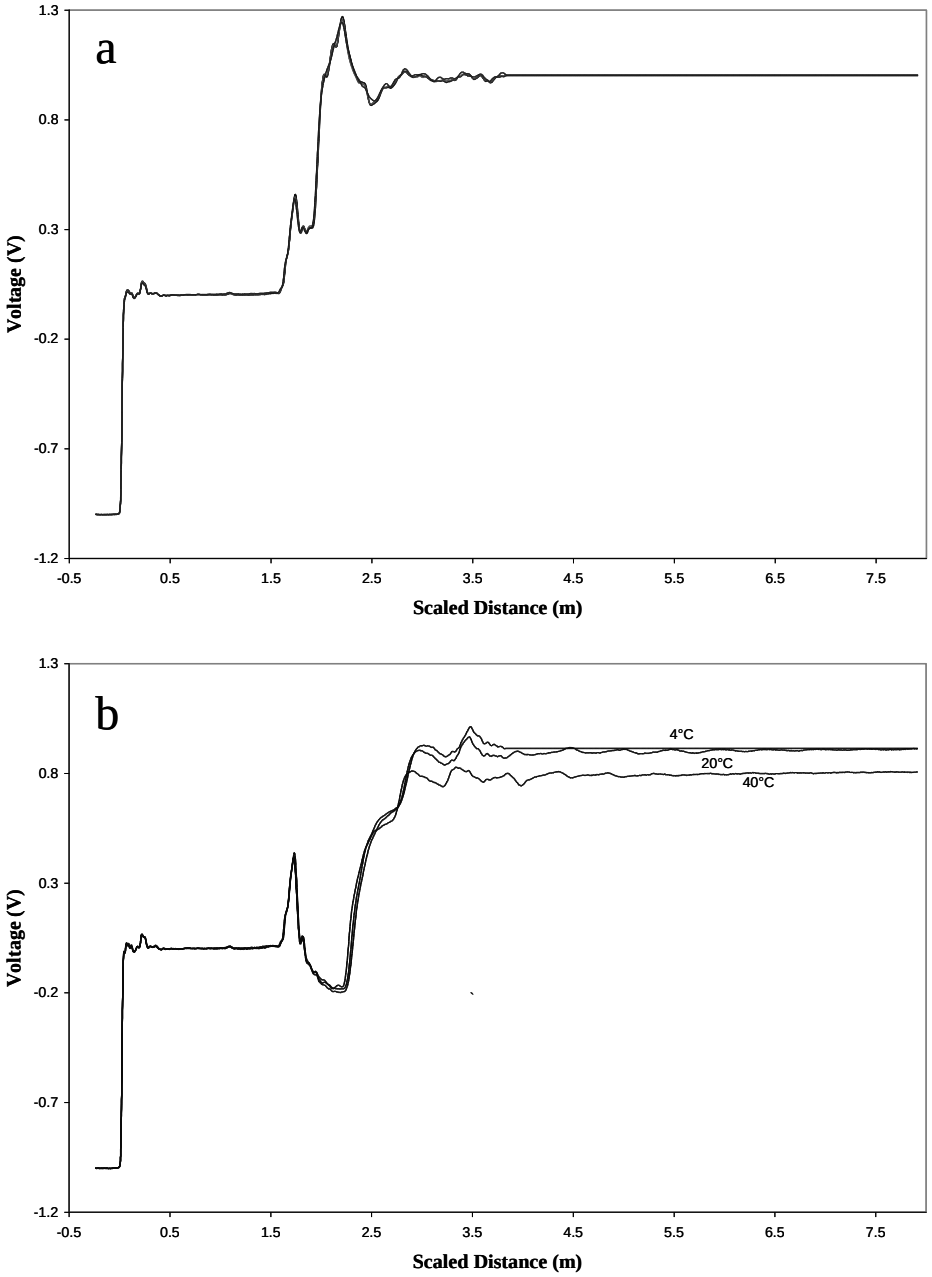

Figure 4-1 TDR waveforms for fine sand a) in a dry natural state b) saturated, temperature ranging from 4°C to 40°C

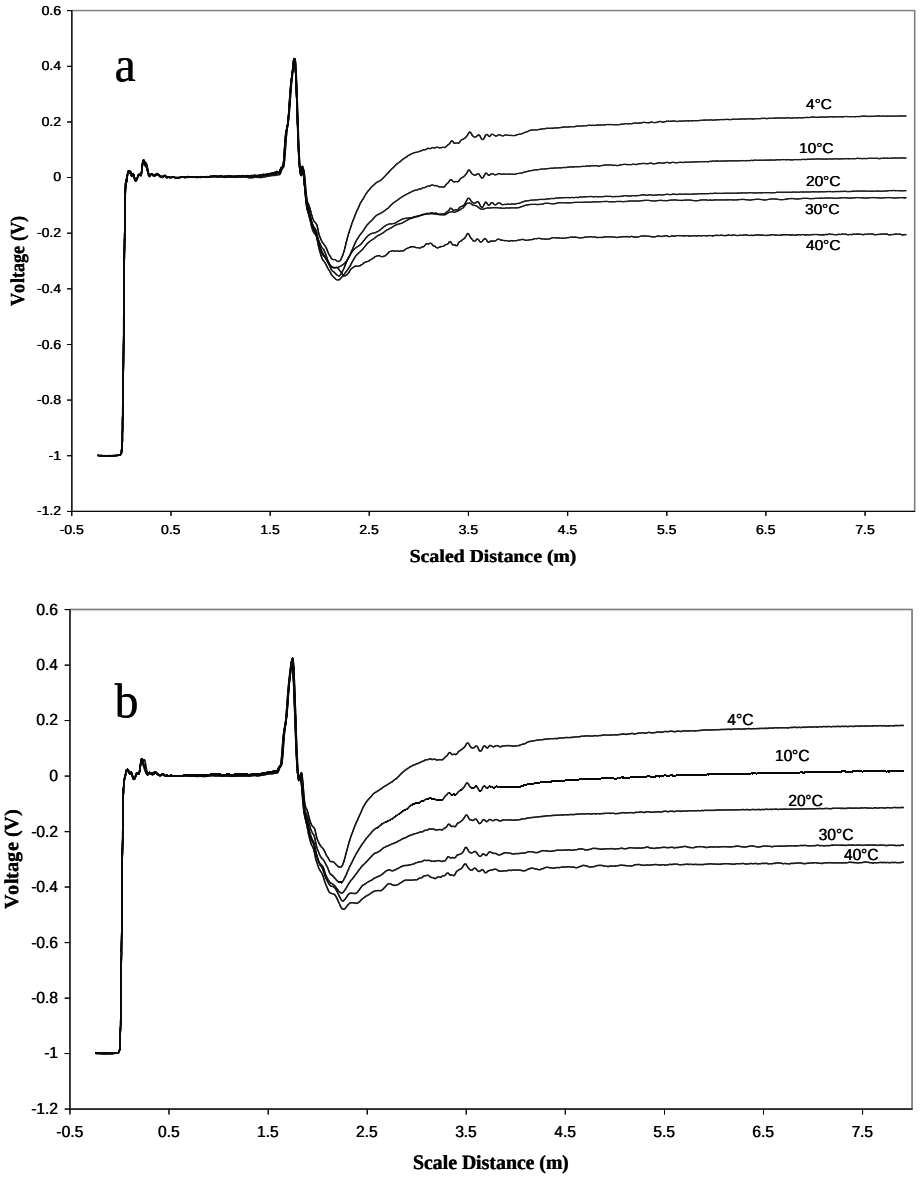

Figure 4-2 TDR waveforms for Crosby till, a) water content = 15%, b) water content = 18%, temperature ranging from 4°C to 40°C

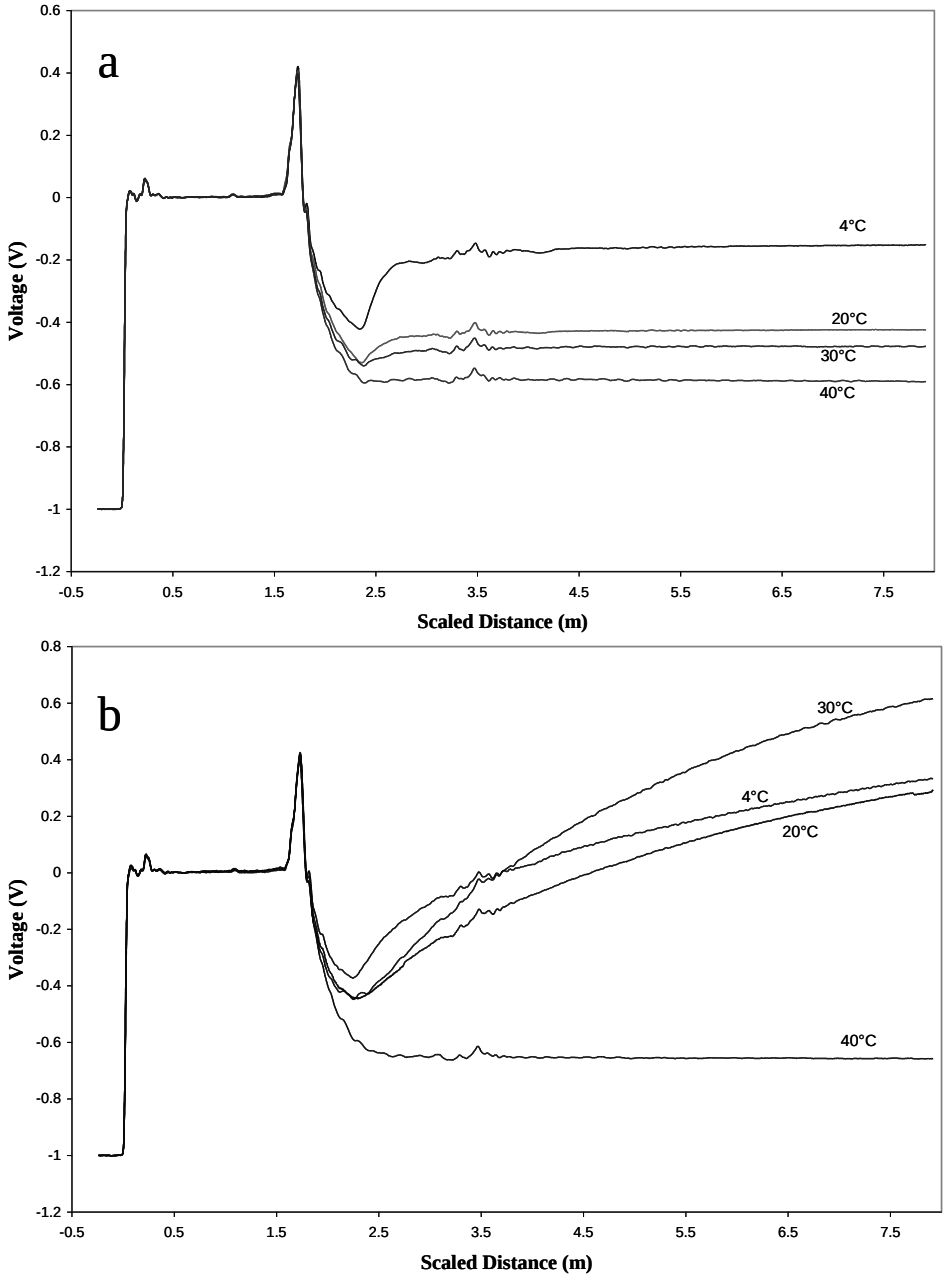

Figure 4-3 TDR waveforms for a) Kaolinite water content = 40%, b) Illite water content = 20%, temperature ranging from 4°C to 40°C

The waveforms for Crosby till are similar to the saturated sands in that there is an obvious decrease in the final voltage as the temperature increases (Figure 4-2). These changes are relatively uniform for the soil at a particular water content, although some

irregularities do occur. As an example, in Figure 4-2a the waveforms for 20°C and 30°C are closer together than Crosby till at a slightly higher water content shown in Figure 4-2b. Kaolinite exhibits this same trend in Figure 4-3a. Unlike the other soils, the waveforms for illite continue to increase as time elapses and the long term voltage does not appear to be reached; therefore, it cannot be accurately estimated. The waveform for 30°C is also abnormal because it jumps above the lower temperatures and measurements are probably not accurate.

4.5.2. Normalized Electrical Conductivity

The normalized electrical conductivity is obtained by dividing the measured values reported in Table 4-1 by the measured electrical conductivity at 20°C for a given soil at the same water content. The results are plotted in Figure 4-4. It is observed that the electrical conductivity increases with increasing temperature for both cohesive and non-cohesive soils. The exception occurs in concrete sand in a dry state, but along with fine sand in a dry state, the changes in electrical conductivity are so slight compared to other soils that it is believed that temperature has little effect on the measurements in these soils. It is likely due to the limited amount of water present in the soil.

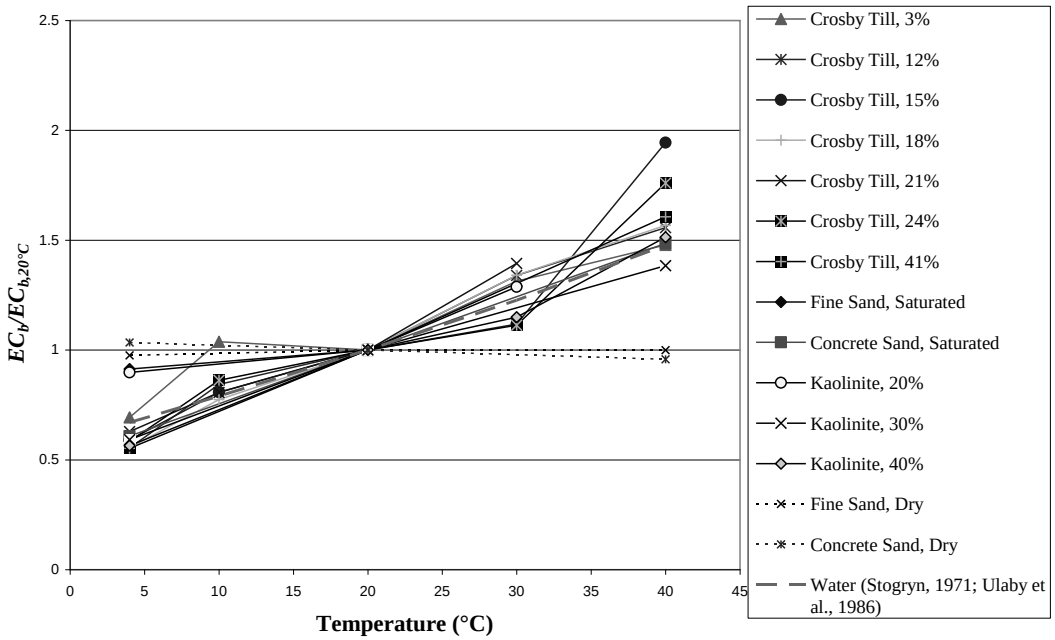

Figure 4-4 Normalized electrical conductivity versus temperature

There is some scatter and inconsistency in the trends for different water contents. The electrical conductivity of Crosby till at water contents of 15% and 24% are higher compared to the other soils at 40°C. Experimental errors and temperature variations during testing could also contribute to fluctuations in the electrical conductivity. To smooth the trends, plots of the electrical conductivity versus temperature were made for each soil and water content. Best fit lines were drawn and equations for the lines were used to calculate approximate values of the electrical conductivity corresponding to each temperature. These values were then normalized to 20°C and plotted in Figure 4-5. It can be observed that when water is present, the trends are independent of soil type. The normalized electrical conductivity of soils increases with increasing temperature within a range of approximately 0.5 to 1.6. The range for normalized electrical conductivity of water is approximately 0.7 to 1.5. Crosby till, water content 3% and kaolinite, water content 20% have a smaller variation in electrical conductivity, which differs from the other soils, as a function of temperature. This could be a result of less water present.

Similar to the observation made by Wraith and Or (1999), the measured electrical conductivity in most cases is higher than EC_b of water at 40°C. The normalized electrical conductivity of water calculated using equation 4.1 is also shown on the plot.

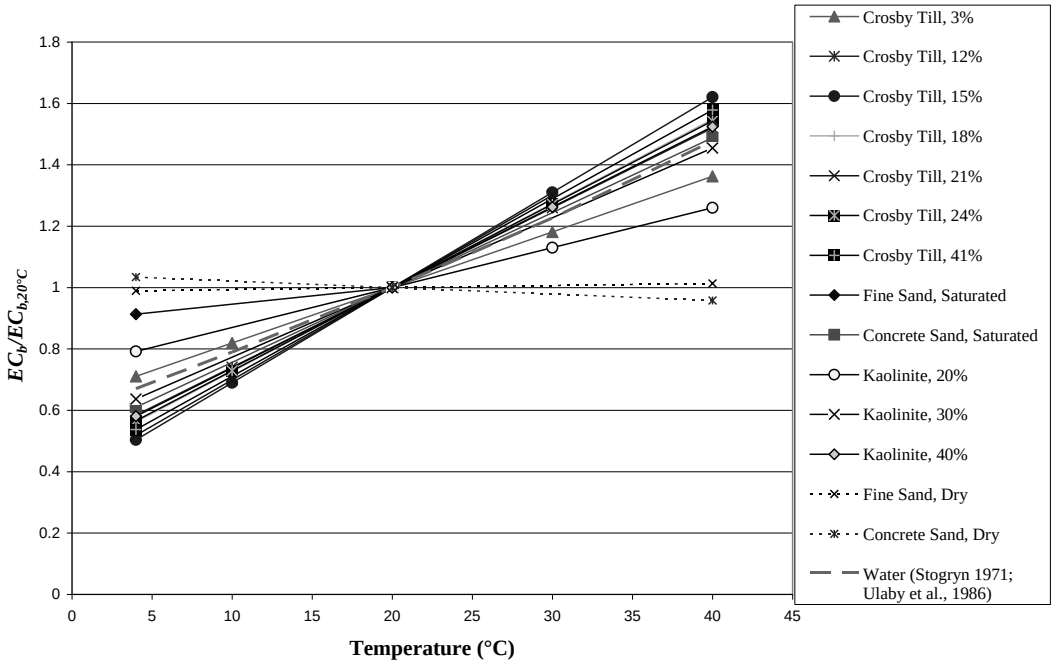

Figure 4-5 Normalized electrical conductivity versus temperature best fit lines through measured electrical conductivity values

4.6. Correction Recommendations

The average of the soils, excluding the dry sands, at each temperature is plotted in Figure 4-6. The best fit line illustrates the temperature correction defined by Equation 4.4. The temperature correction for water is also shown on the plot (Eq. 4.1). The proposed correction is similar to the correction for water. Compared to the values of water, the correction slightly overestimates the electrical conductivity at temperatures above 20°C while underestimating EC_b at temperatures below 20°C. Equation 4.4 can be applied to correct the electrical conductivity for both cohesionless, unless dry and cohesive soils for temperatures between 4°C and 40°C. Variation in the data could also

be a function of the water content of the samples. The electrical conductivity is a function of the flow path of electric currents through the soil. Zambrano (2006) shows that the normalized electrical conductivity has a steeper relationship with water content for values below optimum on a standard compaction curve than above optimum. As water content increases the soils have a higher tortuosity which alters the nature of the flow path.

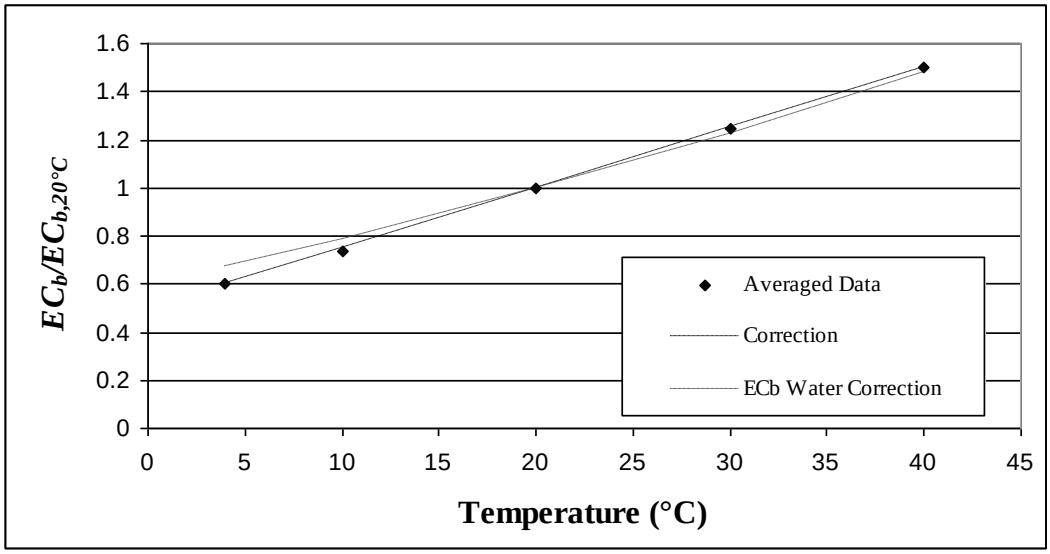

Figure 4-6 Averaged normalized electrical conductivity versus temperature with the proposed new correction and the temperature correction for water (Eq. 4.1)

$$EC_b = EC_{b,20^\circ C}(0.025T_{test,T^\circ C} + 0.5) \qquad \text{Eq. 4.4}$$

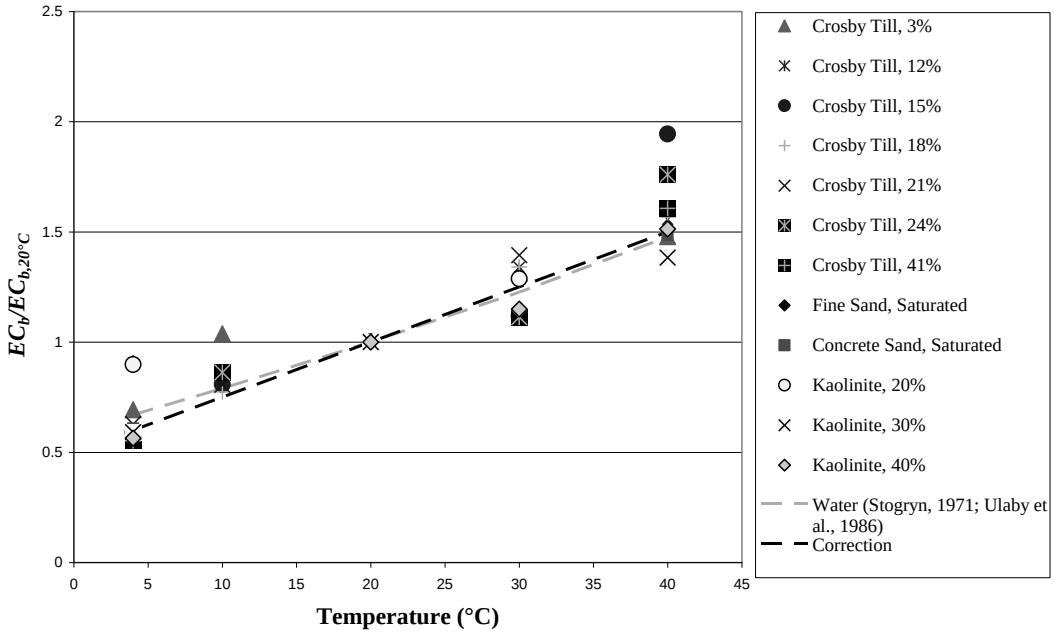

Figure 4-7 Averaged normalized electrical conductivity versus temperature with the proposed new correction and the temperature correction for water (Eq. 4.1)

The gravimetric water content and dry density is related to the electrical conductivity through the calibration equation (4.5) developed by Yu and Drnevich (2004).

$$\sqrt{EC_b}\,\frac{\rho_w}{\rho_d} = c + dw \qquad \text{Eq. 4.5}$$

where c and d are soil-type depended constants, ρ_w is the density of water, and ρ_d is the dry density of the soil.

This relationship is similar to equation 3.11 using the apparent dielectric constant.

CHAPTER 5. PULSE AREA OF A WAVEFORM

5.1. Introduction

The TDR waveforms measured consists of many more points than are actually analyzed in the determination of the apparent dielectric constant and electrical conductivity. It is possible that there is more information that can be extracted from the waveform. Zambrano (2006) proposed measuring the pulse area of the TDR waveform to use as a potential indicator of soil characteristics in addition to improving the estimations of water content and dry density.

5.2. Evaluation of the Pulse Area

As previously discussed, the TDR device applies a step d.c. voltage to the probe. There are two reflections present in the TDR waveform that are used to determine the apparent dielectric constant. The first reflection is caused by an impedance mismatch between the cable and the probe head, the peak occurs when the electromagnetic pulse reaches the soil surface. The beginning of the second reflection occurs when the pulse reflects back from the end of the probes in the soil. This second reflection appears as a rise in the reflected voltage. In soils with particularly high electrical conductivities there can be little or no rise associated with the second reflection

The derivative of the voltage measured yields a pulse for each of the corresponding reflections. Figure 5-1 illustrates the original waveform along with the first derivative of the waveform. The first pulse area is the area under the first derivative curve between the beginning of the reflection due to the probe head and its peak (Figure 5-2 points A and B) which is the beginning of the reflection from the soil surface. The second pulse area is the area under the first derivative between the beginning of the second

reflection and the point of inflection of the waveform which corresponds to the peak of the first derivative (Figure 5-3 points C and D). This area is only a portion of the area associated with the reflection from the end of the rods. It was chosen because it was well defined compared to the area associated with the whole reflection because it takes a long time for the last part of the curve to return to a horizontal asymptote (zero value of the derivative).

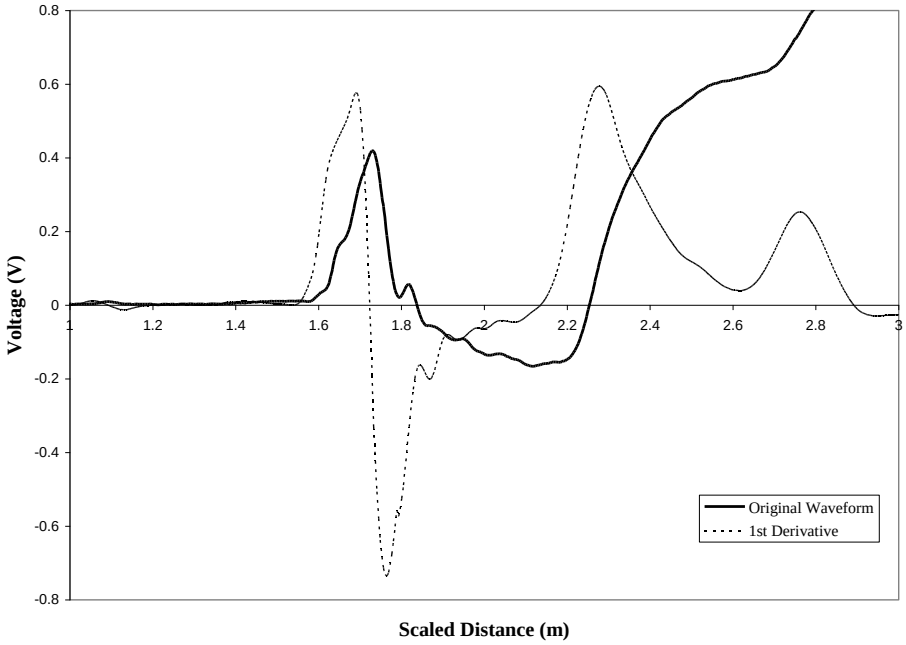

Figure 5-1 Saturated concrete sand TDR waveform and the first derivative

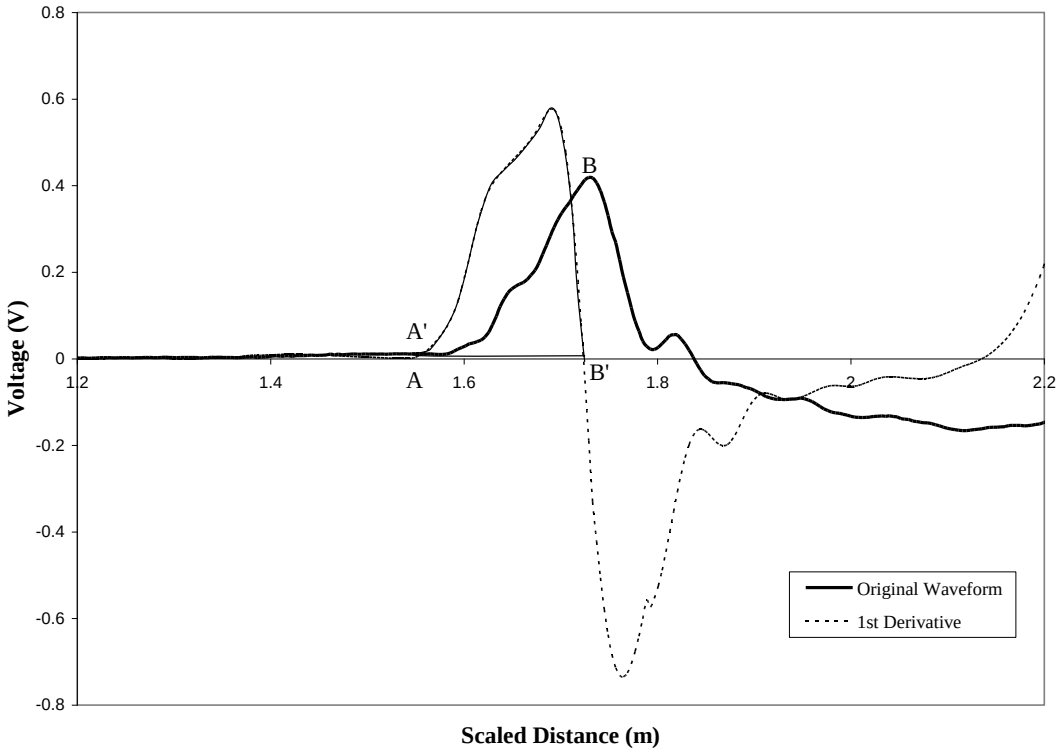

Figure 5-2 Pulse area of the first reflection (shaded region), point A is the beginning of the reflection, point A' is the beginning of the first derivative, point B is the peak of the reflection, and point B' is the zero crossing of the first derivative due to the peak in the reflection

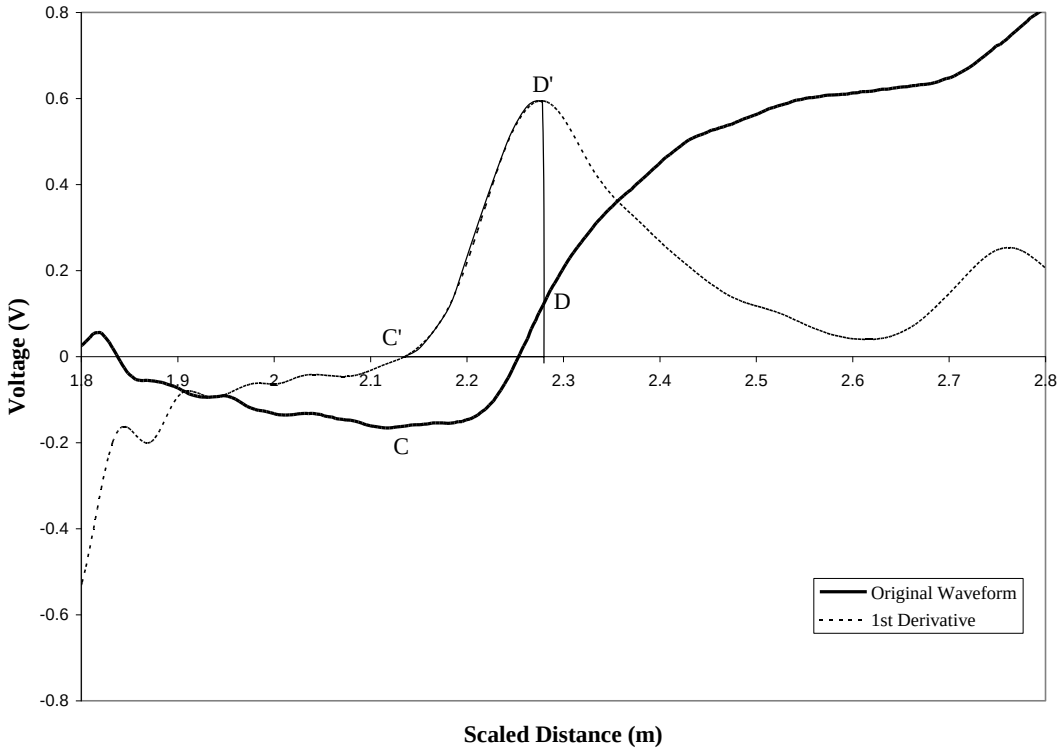

Figure 5-3 Pulse area of part of the second reflection, point C is the beginning of the reflection, point C' is the zero of the first derivative due to the beginning of the reflection, point D is the inflection point of the reflection, and point D' is the peak of the first derivative due to the inflection point of the reflection

For the pulse area described in Fig. 5-2, the area under the first derivative curve between A' and B'; when integrated it is equal to the voltage difference between the two points on the original waveform, A and B. The first pulse area is important to characterize the input voltage by the TDR device and effects of the probe head on the signal. It was hypothesized that for a given TDR device, cable, and probe head that this area will be relatively constant. However, the peak of the first reflection occurs when the pulse reaches the soil surface; therefore, the location and amplitude of the peak of the signal could be influenced by the soil type.

For the pulse area described in Fig. 5-3, the derivative usually gives a pulse whose area is not easily defined, especially for the portion past the peak of the derivative.

Hence, only the area of the pulse to the peak is used and this pulse area is equal to the difference in voltage of the original curve between point D and C (Figure 5-3).

5.3. Test Results

The PMTDR SM software used to evaluate the soil data for the apparent dielectric constant and electrical conductivity could not be used to compute the pulse areas because it does not identify the inflection point of the second reflection. A TDR Analysis program was developed by Murty Malladi in July 2006 which, similar to PMTDR SM, uses curve fitting and derivatives to identify the four points needed to compute the pulse areas. It also reports values for the electrical conductivity and apparent dielectric constant. Further testing of the algorithm is needed before it can be reliably used to estimate K_a and EC_b for all soils. A lot of scatter is expected in the pulse area data, mostly in the pulse area of the second reflection, due to noise in the signal leading to misinterpretation of the waveforms and irregularities caused by the smoothing derivative functions in the computer program. Table 5-1 presents the results from the analysis of the data using the TDR Analysis program.

Table 5-1 Pulse area of the first (PA, 1st) and second (PA 2nd) reflections

Soil	Target Water Content (%)	Pulse Area	Temperature (°C)				
			4	10	20	30	40
Crosby Till	3	PA, 1st	0.462	0.456	0.448	0.443	0.438
		PA, 2nd	0.179	0.157	0.129	0.124	0.106
	12	PA, 1st	0.436	0.427	0.426	0.417	0.419
		PA, 2nd	0.073	0.026	0.067	0.044	0.031
	15	PA, 1st	0.431	0.425	0.419	0.414	0.411
		PA, 2nd	0.049	0.030	-0.016	0.024	0.018
	18	PA, 1st	0.430	0.424	0.414	0.407	0.412
		PA, 2nd	0.051	0.029	0.008	0.024	0.011
	21	PA, 1st	0.427	0.422	0.418	0.406	0.417
		PA, 2nd	0.041	0.027	0.012	0.000	0.000
	24	PA, 1st	0.426	0.421	0.419	0.405	0.412
		PA, 2nd	0.041	0.024	0.021	0.097	0.021
	41	PA, 1st	0.431		0.416		0.404
		PA, 2nd	0.075		0.035		0.016
Illite	20	PA, 1st	0.428		0.415	0.403	0.398
		PA, 2nd	-0.018		0.200	0.123	0.023
	50	PA, 1st	0.426		0.408	0.403	0.401
		PA, 2nd	-0.017		0.029	0.066	0.206
Kaolinite	20	PA, 1st	0.414		0.417	0.403	0.409
		PA, 2nd	0.029		0.005	0.021	0.252
	30	PA, 1st	0.431		0.416		0.404
		PA, 2nd	0.032		-0.016		0.015
	40	PA, 1st	0.425		0.411	0.403	0.401
		PA, 2nd	0.032		-0.016	0.027	0.013
Concrete Sand	dry	PA, 1st	0.152		0.121		-2.405
		PA, 2nd	0.000		0.000		0.000
	saturated	PA, 1st	0.430		0.414		0.406
		PA, 2nd	0.161		0.179		0.143
Fine Sand	dry	PA, 1st	1.107		1.071		1.071
		PA, 2nd	0.312		0.277		0.000
	saturated	PA, 1st	0.433		0.420		0.409
		PA, 2nd	0.180		0.161		0.148

5.4. Temperature Effects on the Pulse Area

The same probe head was used to test all of the soils analyzed in this investigation (described in section 3.3). The first reflection is primarily a function of the cable-probe

head impedance mismatches. The pulse area of the first reflection is should be unaffected by the soil type and water content. Any temperature effects are expected to be a function of the equipment sensitivity and major scatter in the data is not expected. The pulse area of the second reflection; however, is expected to exhibit significant scatter because of the difficulty in identifying the beginning and inflection point of the reflection. Also as discussed previously the second reflections are less discernible in cohesive soils due to higher electrical conductivities compared to non-cohesive soils.

5.4.1. Pulse Area of the First Reflection

The normalized pulse area of the first reflection is obtained by dividing the measured values reported in Table 5-1 by the measured pulse area at 20°C for a given soil at the same water content. The results are plotted in Figure 5-4. The pulse area of all the soils decreases with increasing temperature with the exception of kaolinite at 20% water content. This point appears to be the only exception to the trend and could possibly be caused by an error in the analysis of the waveforms by the TDR Analysis program or the waveforms themselves could have had noise interference. In a few soils, the pulse area increases between 30°C and 40°C. These irregularities could be a result of experimental error and errors in analysis by the computer algorithm. The changes in normalized pulse area of the first reflection are relatively small and range from approximately 1.04 to 0.96.

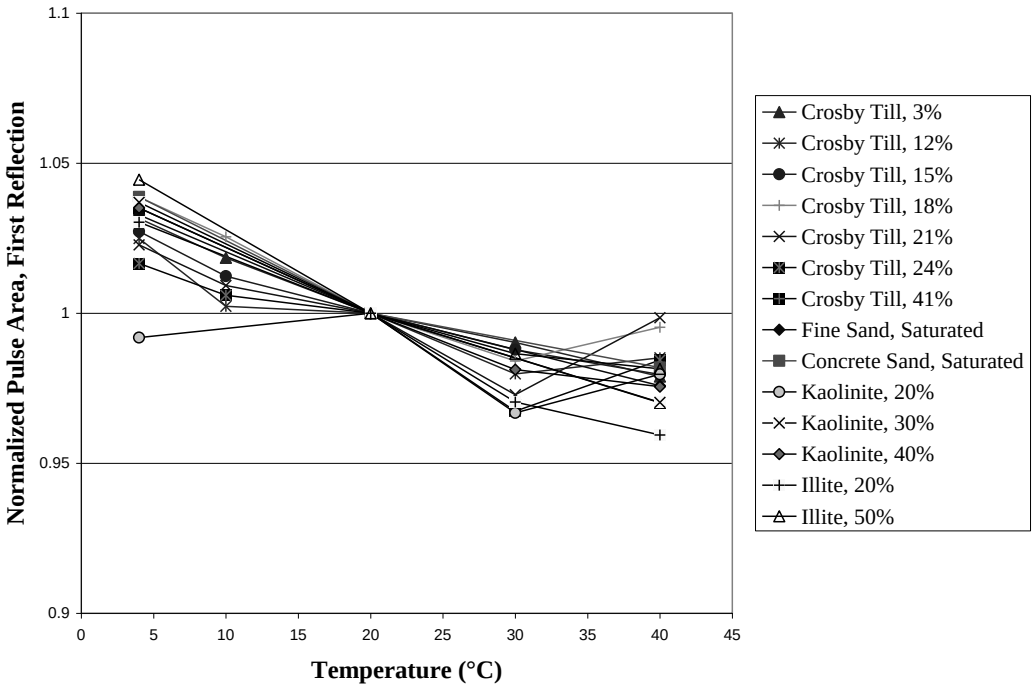

Figure 5-4 Normalized pulse area of the first reflection versus temperature

To smooth out the irregular data best fit curves were fitted to plots of the normalized pulse area versus temperature for each soil and water content. The results are plotted in Figure 5-5. It can be observed that the oscillations as temperature increases have been eliminated without significantly altering the range of variation with changing temperature. The pulse area of the first reflection based on the best fit lines varies from approximately 1.03 to 0.96.

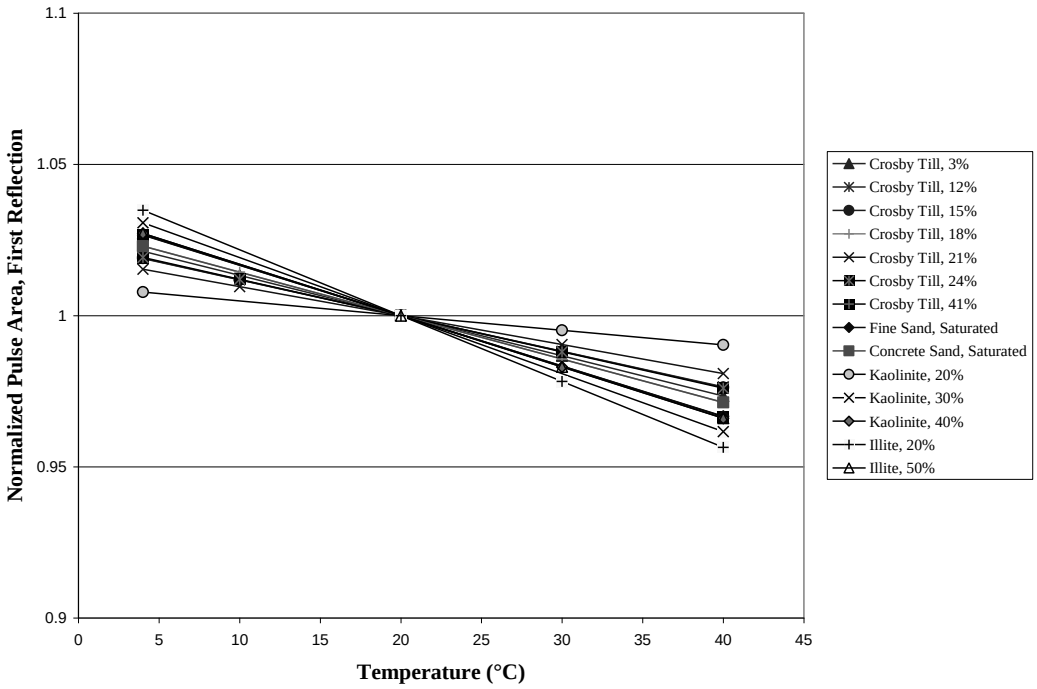

Figure 5-5 Normalized pulse area of the first reflection versus temperature of calculated values based on the best fit lines for each soil and water content

5.4.2. Pulse Area of the Second Reflection

The normalized pulse area of the second reflection is obtained by dividing the measured values reported in Table 5-1 by the measured pulse area at 20°C for a given soil at the same water content. The results are plotted in Figure 5-6. Generally it appears that the pulse area decreases as the temperature increases. As expected there is significant scatter in the calculated pulse areas. The most obvious irregularities occur in kaolinite, water content 20% and Crosby tills, water contents 18%, 21%, and 24%.

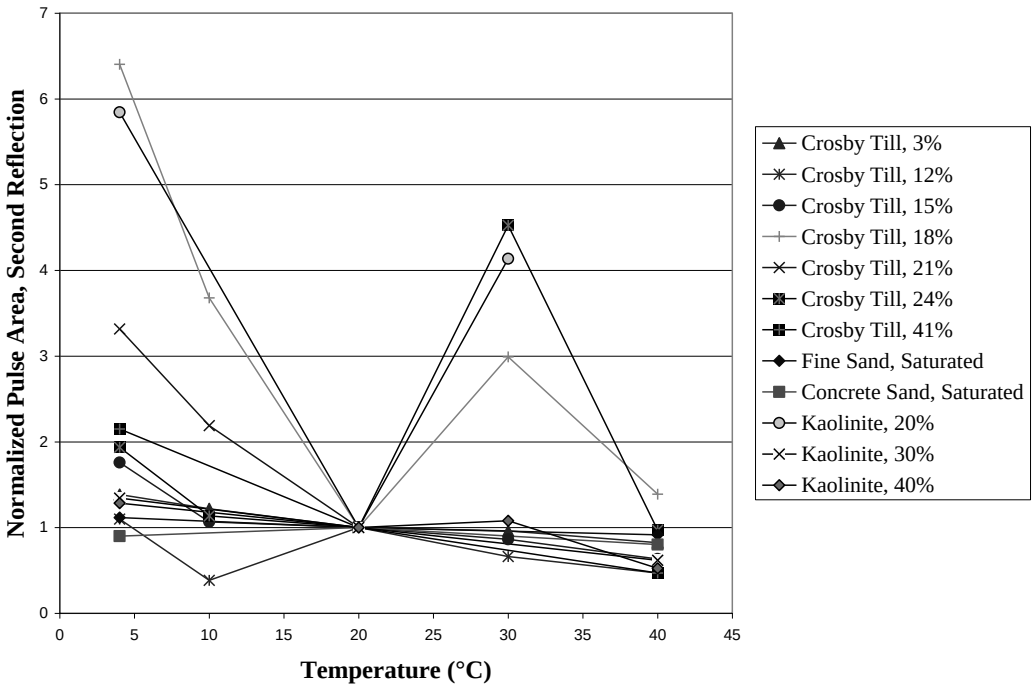

Figure 5-6 Normalized pulse area of the second reflection versus temperature

Figure 5-7 isolates the irregular data sets kaolinite, water content 20% and Crosby tills, water contents 18%, 21%, and 24%. Kaolinite, water content 20% and Crosby till, water content 18% appear to have erroneous calculated pulse areas at 20°C which alter the normalized pulse area. These points were discarded and best fit lines were fit through the remaining points resulting in trends more consistent with the rest of the data; however, there is still uncertainty that the best fit line is a true representation of the behavior of these soils at this water content. If the option was available, more testing would have been performed on these soils to investigate these irregularities. Because of the uncertainty in the validity of this data it was disregarded for the remainder of the analysis. For Crosby till, water content 24%, the calculated pulse area at 30°C is significantly larger than the other temperatures. This value is obviously erroneous, possibly caused by an error in the location of the points by the TDR Analysis program and was discarded. The best fit line was fit through the remaining data points. Crosby till, water content 21% consists of only three points corresponding to temperatures of 4°C,

10°C, and 20°C. Although based on the trends of the other soils it could be assumed that the pulse area would decrease as the temperature continues to increase, but there is no certainty that these normalized values are correct. The calculated pulse area at 20°C could be erroneous which could explain the large variation in normalized pulse area. Without the aide of at least one point from a temperature greater than 20°C, best fit trends through the data may not be a true representation and therefore this set of data was discarded for the remainder of the analysis.

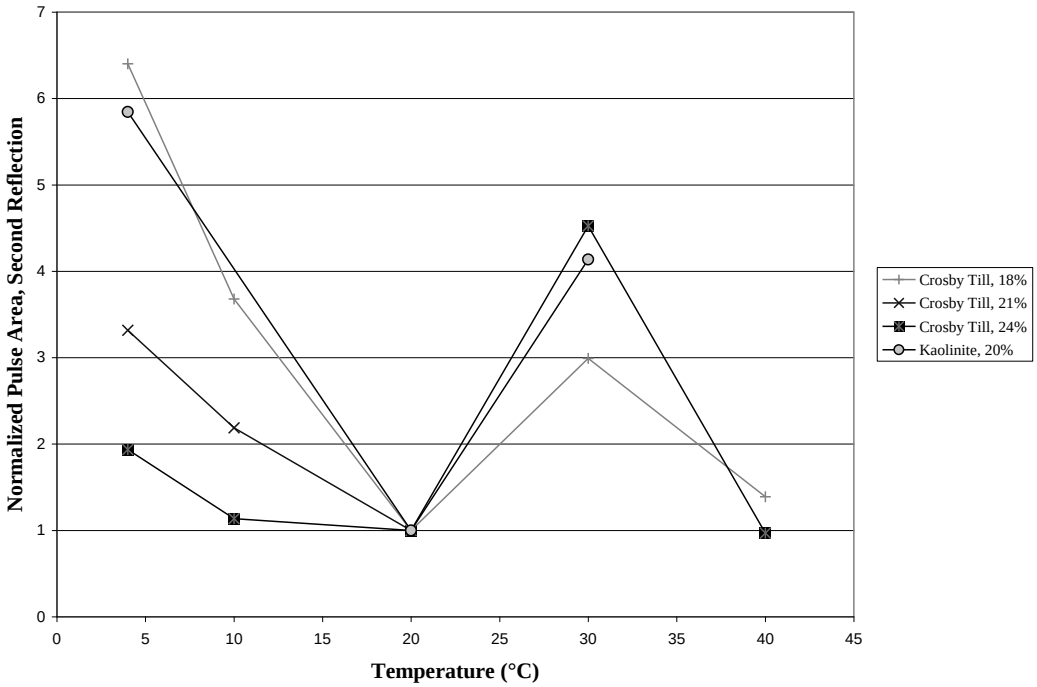

Figure 5-7 Normalized pulse area of the second reflection versus temperature, irregular trends

Figure 5-8 shows the remaining data which exhibits clearer trends and relatively smaller oscillations with increasing temperatures. This scatter is easily smoothed using best fit lines fitted through plots of the normalized pulse area versus temperature. The results from the linear curve fit of the data are presented in Figure 5-9. It is interesting to note that the non-cohesive sands tend to have a smaller variation of the pulse area with

increasing temperature than the cohesive soils. The non-cohesive soils range from approximately 1.09 to 0.9 and the cohesive soils mostly range from approximately 1.35 to 0.55, except for Crosby till, water content 41% which has a larger variation from approximately 1.6 to 0.27. This difference could be caused by the relatively high water content of the soil.

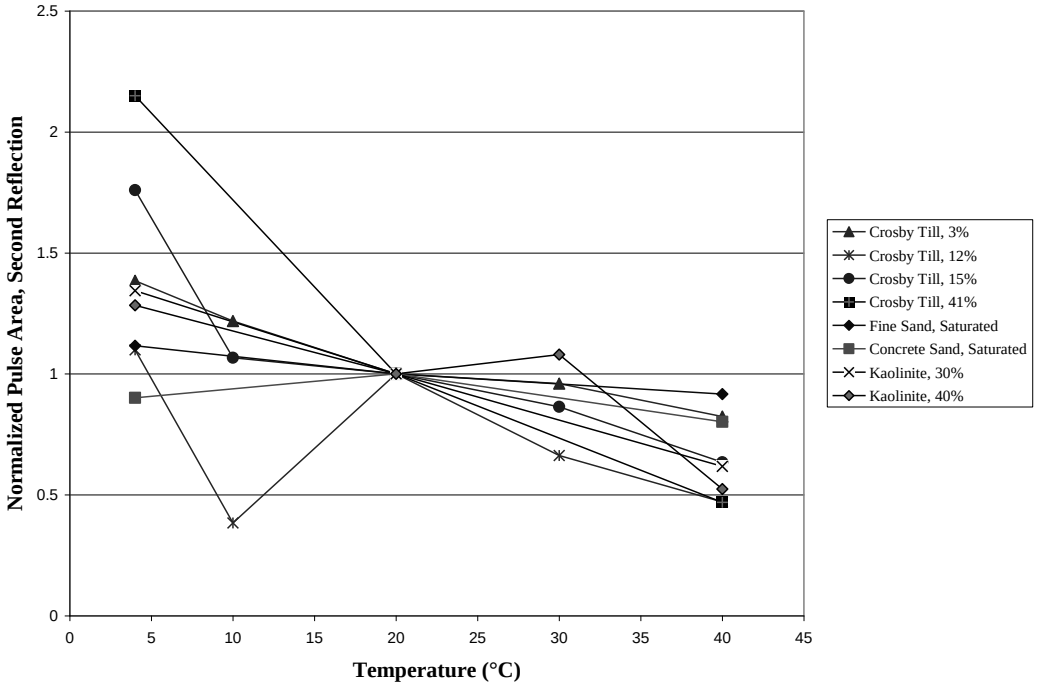

Figure 5-8 Normalized pulse area of the second reflection versus temperature

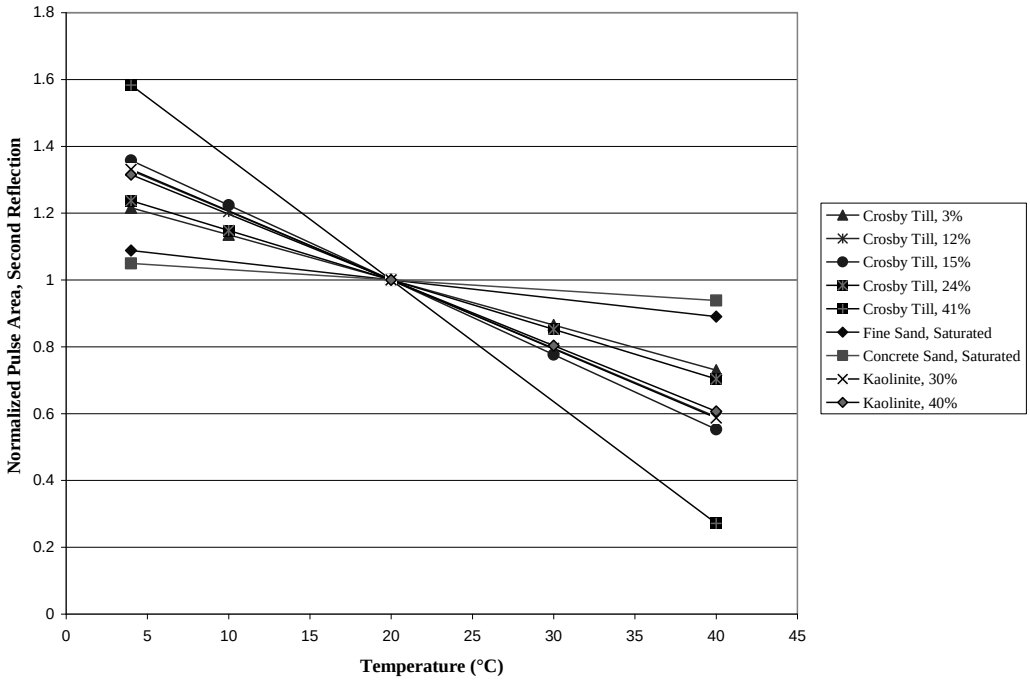

Figure 5-9 Normalized pulse area of the second reflection versus temperature of calculated values based on the best fit lines for each soil and water content

5.4.3. Normalized Combined Pulse Area

The normalized combined pulse area is calculated by dividing the pulse area of the second reflection by the pulse area of the first reflection. These values are then divided by the calculated values at 20°C. The results are plotting in Figure 5-10. The pulse area of the first reflection is dependent on the probe head used to perform the TDR test which implies different pulse areas would be calculated for different probe heads. By dividing the pulse area of the second reflection by the pulse area of the first reflection, the area is normalized to account for the type of probe head used.

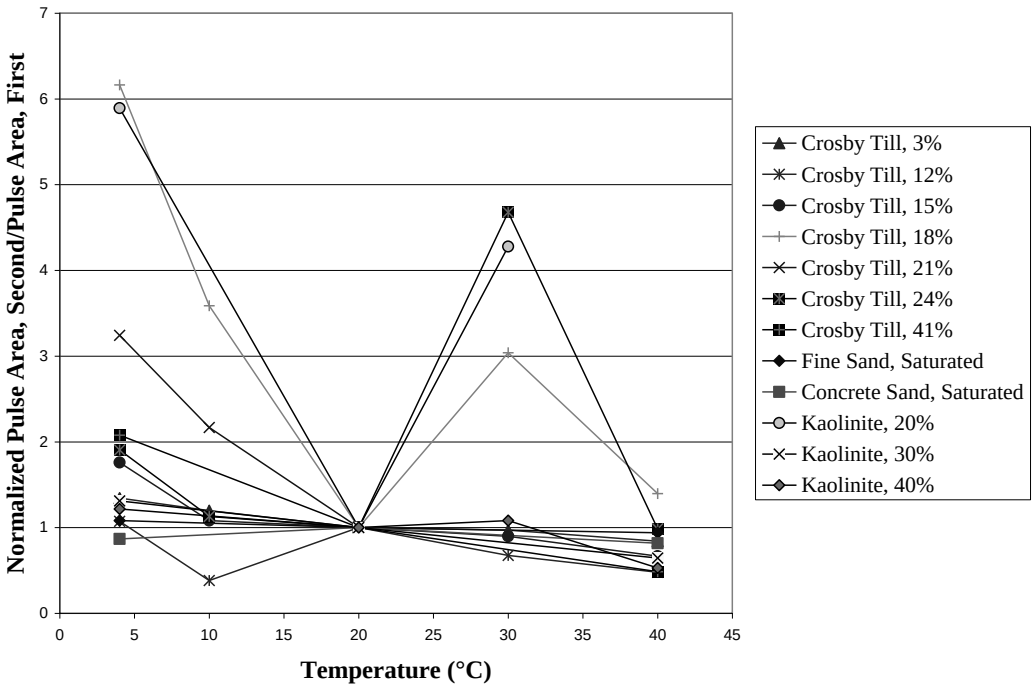

Figure 5-10 Normalized combined pulse area versus temperature

Because there is very little variation with temperature of the pulse area of the first reflection, the trends for the normalized combined pulse area appear identical to those of the pulse area of the second reflection. The pulse areas tend to decrease as the temperature increases and the most obvious irregularities occur in kaolinite, water content 20% and Crosby tills, water contents 18%, 21%, and 24%. These irregularities are highlighted in Figure 5-11 and the remaining relatively cleaner data is shown in Figure 5-12. Since we are using the same data, the same logic was applied to these trends and the values of normalized combined pulse area of kaolinite, water content 20% and Crosby till, water content 18% were discarded as well as the value for Crosby till, water content 24% at 30°C. The Crosby till, water content 21% was also excluded from further analysis because not enough information can be obtained from the three points to make a true assessment of the behavior of this soil at this water content.

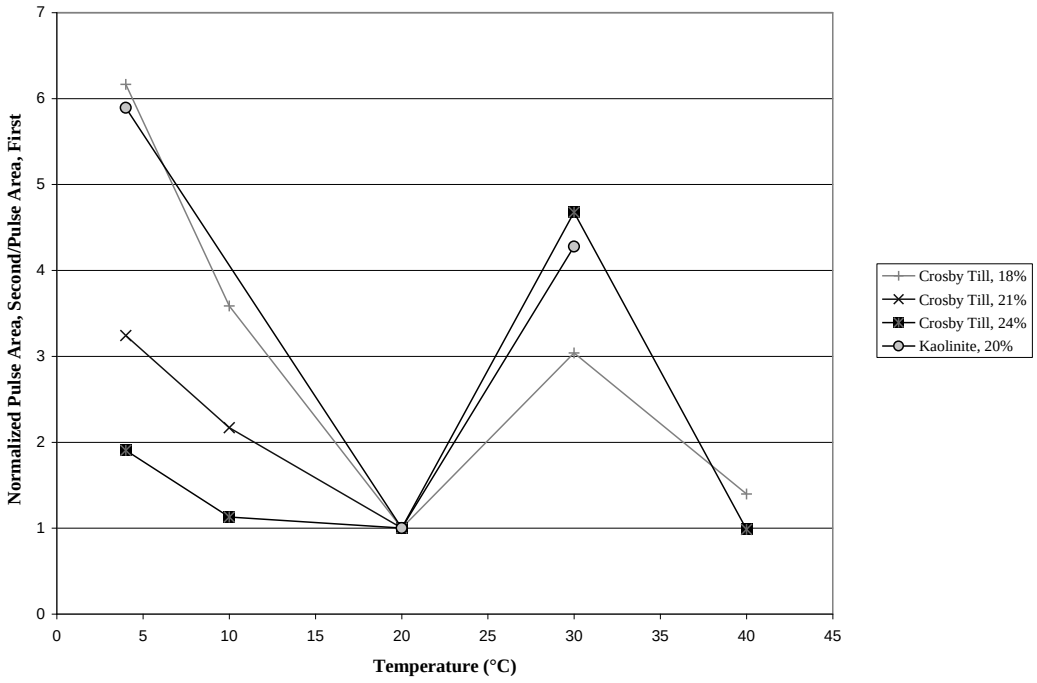

Figure 5-11 Normalized combined pulse area versus temperature, irregular trends

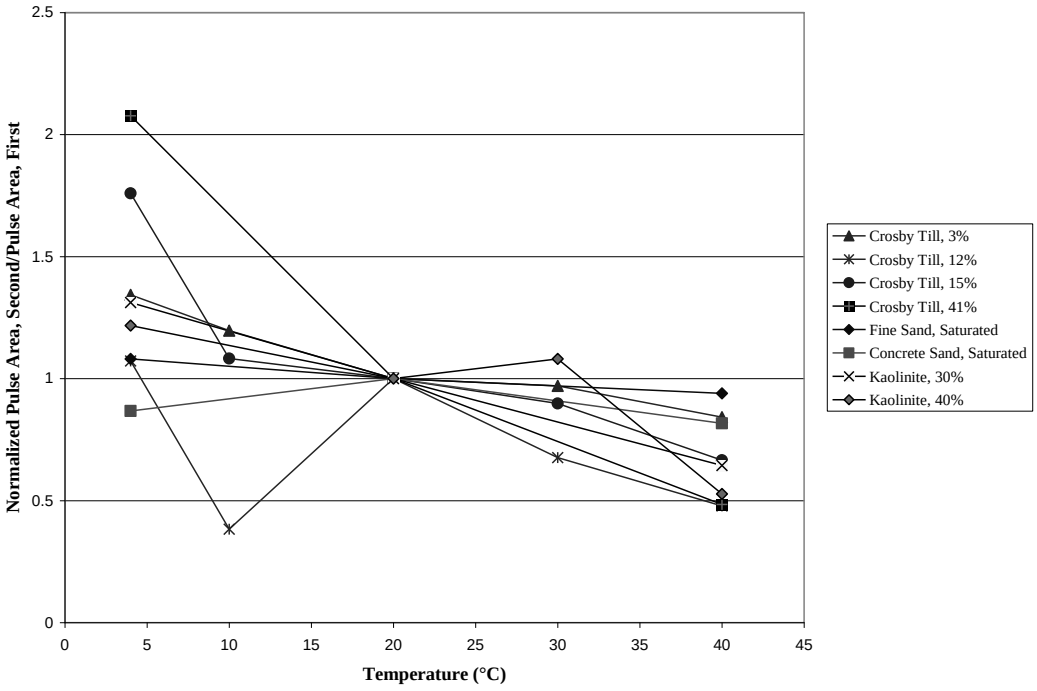

Figure 5-12 Normalized combined pulse area versus temperature

The best fit trends associated with all of the soils are plotted in Figure 5-13. Again the same trends are observed for the normalized combined pulse area and the pulse area of the second reflection. The ranges of variation for both non-cohesive and cohesive soils are slightly lower at colder temperatures and remain relatively unchanged at warmer temperatures. The non-cohesive soils range from approximately 1.06 to 0.9 and the cohesive soils range from approximately 1.5 to 0.3.

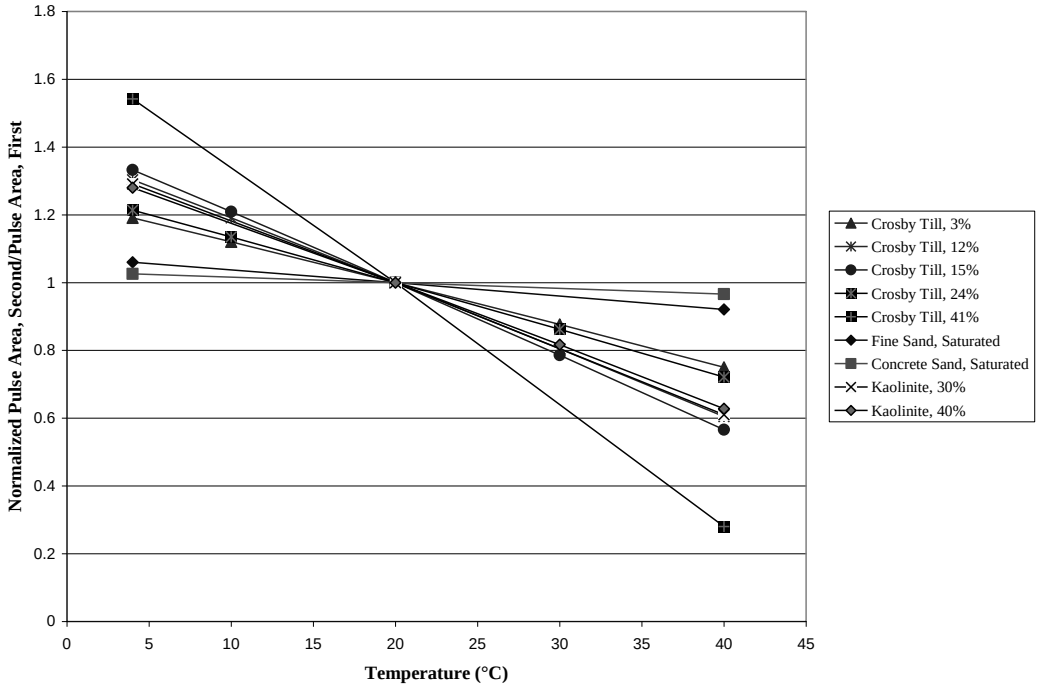

Figure 5-13 Normalized combined pulse area versus temperature of calculated values based on the best fit lines for each soil and water content

5.5. Correction Recommendations

The average of the pulse area of the first reflection for all soils is plotted in Figure 5-14. The dashed correction line (Eq. 5.1) is based on the best fit line through these points. Figure 5-15 shows this correction along with the actual calculated values of the pulse area of the first reflection. The correction generally underestimates the pulse area at

4°C and overestimates the pulse area at 40°C; however, the expected error is within approximately +/- 2%.

$$PA_{1^{st}} = PA_{1^{st},20^{\circ}C} \cdot (1.028 - 0.0014 T_{test,^{\circ}C}) \qquad \text{Eq. 5.1}$$

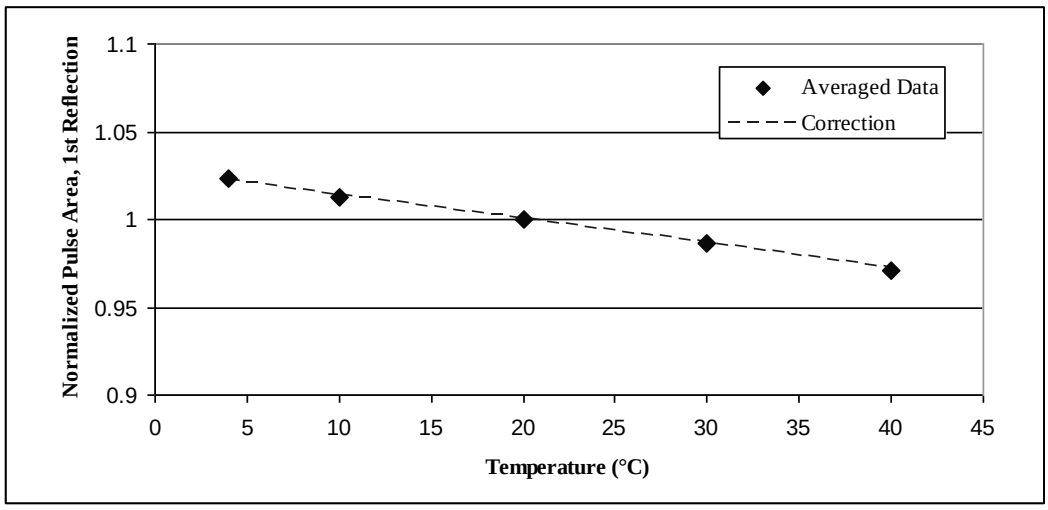

Figure 5-14 Averaged normalized pulse area of the first reflection versus temperature with proposed correction

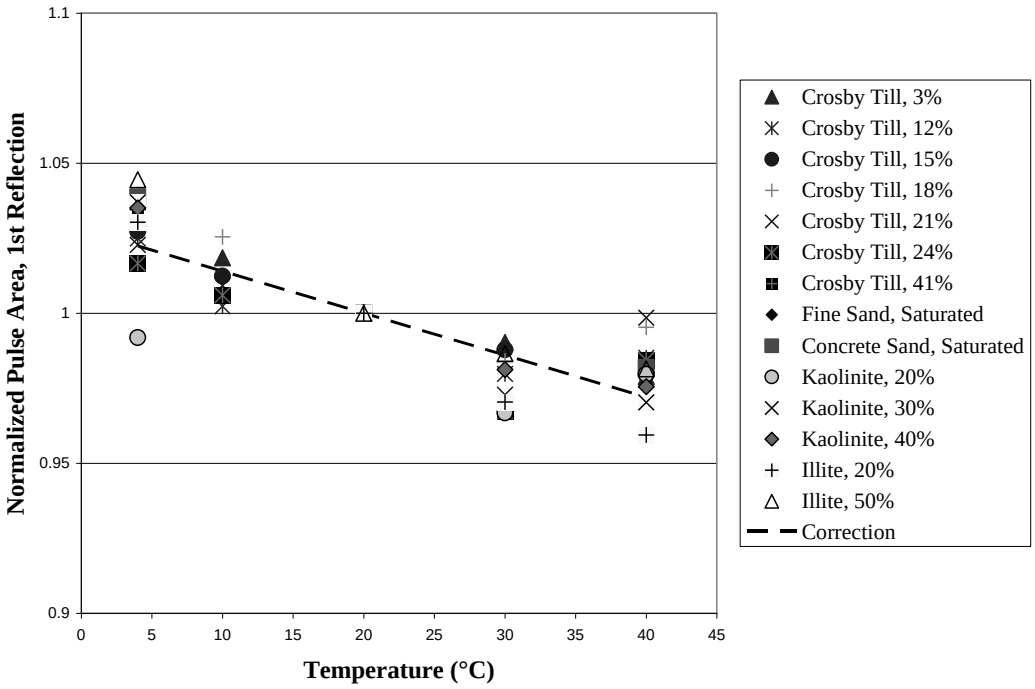

Figure 5-15 Calculated normalized pulse area of the first reflection versus temperature with proposed correction

The averaged pulse area of the second reflection is plotted in Figure 5-16. The cohesionless and cohesive soils were analyzed separately because as mentioned earlier, the cohesionless soils have a smaller variation in pulse area as the temperature increases. Corrections (Eq. 5.2 and Eq. 5.3) based on the best fit lines through these points are also illustrated on the plot. Figure 5-17 shows the correction for cohesionless soils with the actual calculated values of the pulse area from the TDR Analysis program. The correction appears to be valid; however, only two soils are represented. More testing is needed before this correction can be implemented. Figure 5-18 shows the correction for cohesive soils with the actual calculated values of the pulse area of the second reflection excluding the discarded data. There are still a few outlying points, notably Crosby till, water content 12% at 30°C as well as a large amount of scatter at 4°C.

$$PA_{2^{nd}} = PA_{2^{nd},20^{\circ}C} \cdot (1.086 - 0.0043T_{test,^{\circ}C}) \quad \text{cohesionless soils} \qquad \text{Eq. 5.2}$$

$$PA_{2^{nd}} = PA_{2^{nd},20^{\circ}C} \cdot (1.4 - 0.02T_{test,^{\circ}C}) \quad \text{cohesive soils} \qquad \text{Eq. 5.3}$$

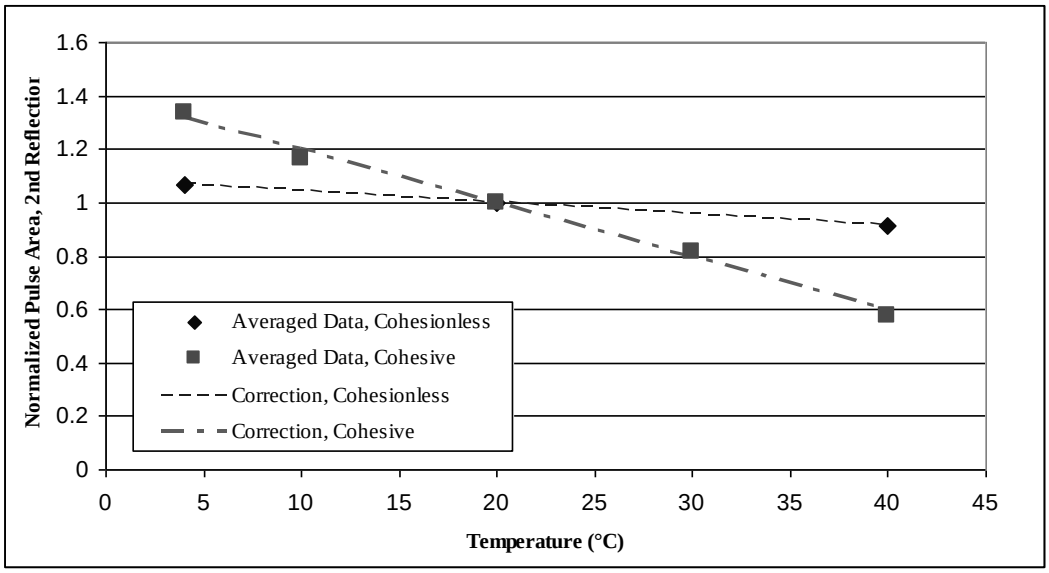

Figure 5-16 Averaged normalized pulse area of the second reflection versus temperature with proposed corrections for both cohesive and non-cohesive soils

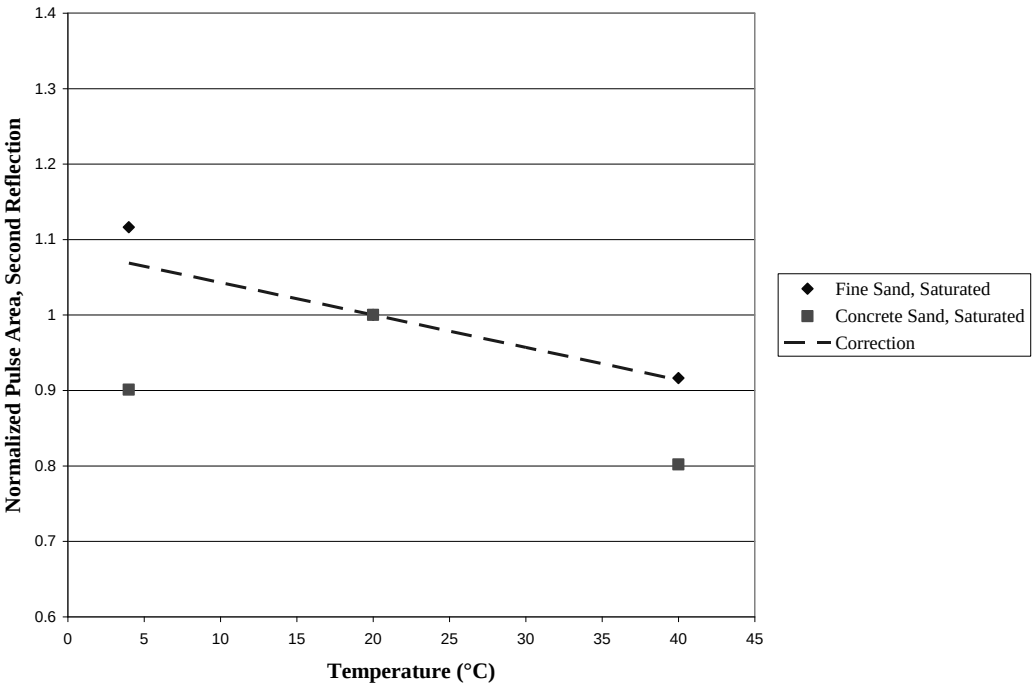

Figure 5-17 Normalized pulse area of the second reflection versus temperature with proposed correction for cohesionless soils

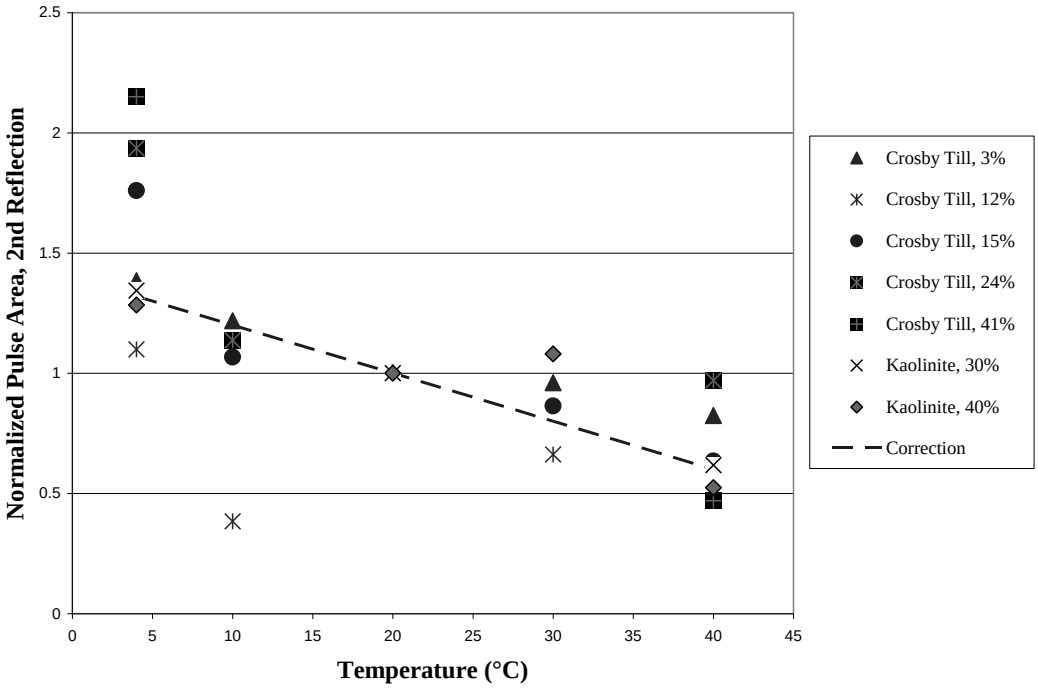

Figure 5-18 Normalized pulse area of the second reflection versus temperature with proposed correction for cohesive soils

The averaged pulse area of the combined pulse area is plotted in Figure 5-19. Because of the similarities with the pulse area of the second reflection the cohesionless and cohesive soils were analyzed separately. Corrections (Eq. 5.4 and Eq. 5.5) based on the best fit lines through these points are also illustrated on the plot. Figure 5-20 shows the correction for cohesionless soils with the actual calculated values of the combined pulse area. The trend is very similar to the pulse area of the second reflection, but as previously mentioned only two soils are represented and more testing is needed before this correction can be implemented. Figure 5-21 shows the correction for cohesive soils with the actual calculated values of the pulse area of the second reflection excluding the discarded data. The plot is almost identical to Figure 5-18 and the correction for cohesive soils is the same as noted in Equation 5.3. The corrections needed for the pulse area second reflection are so much larger than those proposed for the pulse area of the first reflection that when combined, the influence of the temperature on the second reflection is unaffected by the first.

$$PA_{2^{nd}} / PA_{1^{st}} = PA_{2^{nd},20^{\circ}C} / PA_{1^{st},20^{\circ}C} \cdot (1.056 - 0.0028T_{test,^{\circ}C}) \text{ cohesionless soils} \quad \text{Eq. 5.4}$$

$$PA_{2^{nd}} / PA_{1^{st}} = PA_{2^{nd},20^{\circ}C} / PA_{1^{st},20^{\circ}C} \cdot (1.4 - 0.02T_{test,^{\circ}C}) \text{ cohesive soils} \quad \text{Eq. 5.5}$$

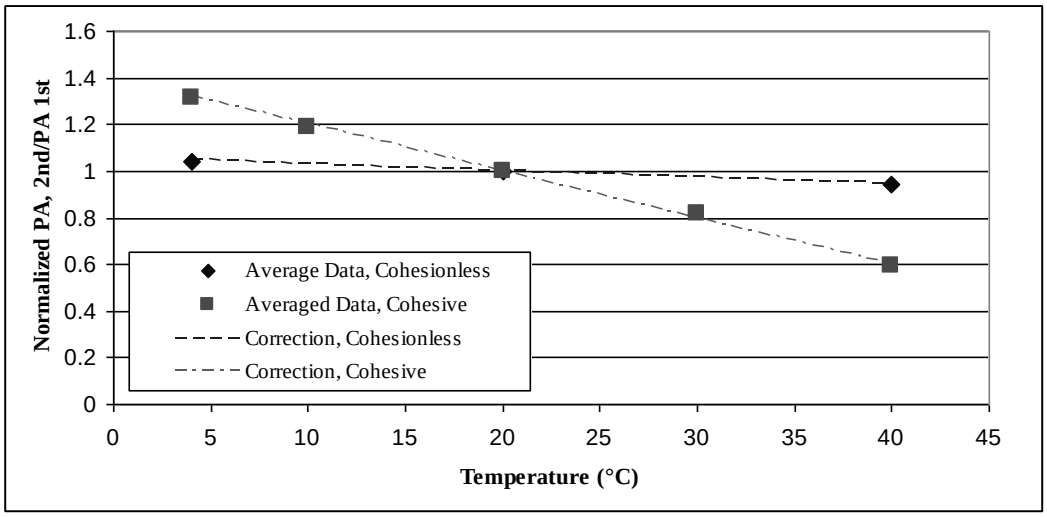

Figure 5-19 Averaged normalized combined pulse area versus temperature with proposed corrections for both cohesive and non-cohesive soils

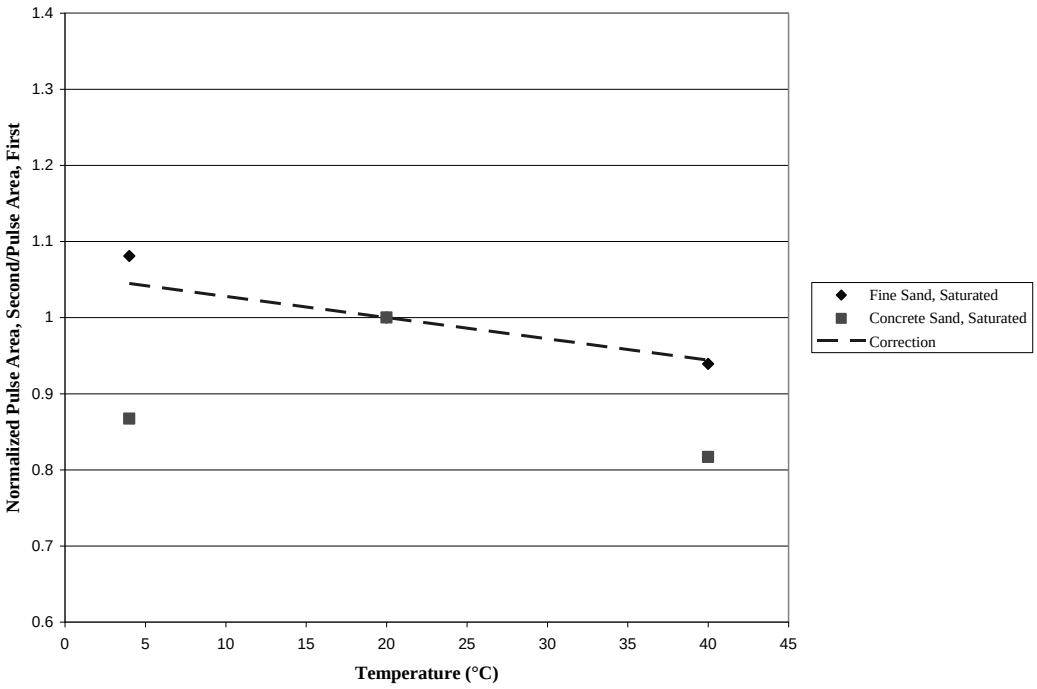

Figure 5-20 Normalized combined pulse area versus temperature with proposed correction for cohesionless soils

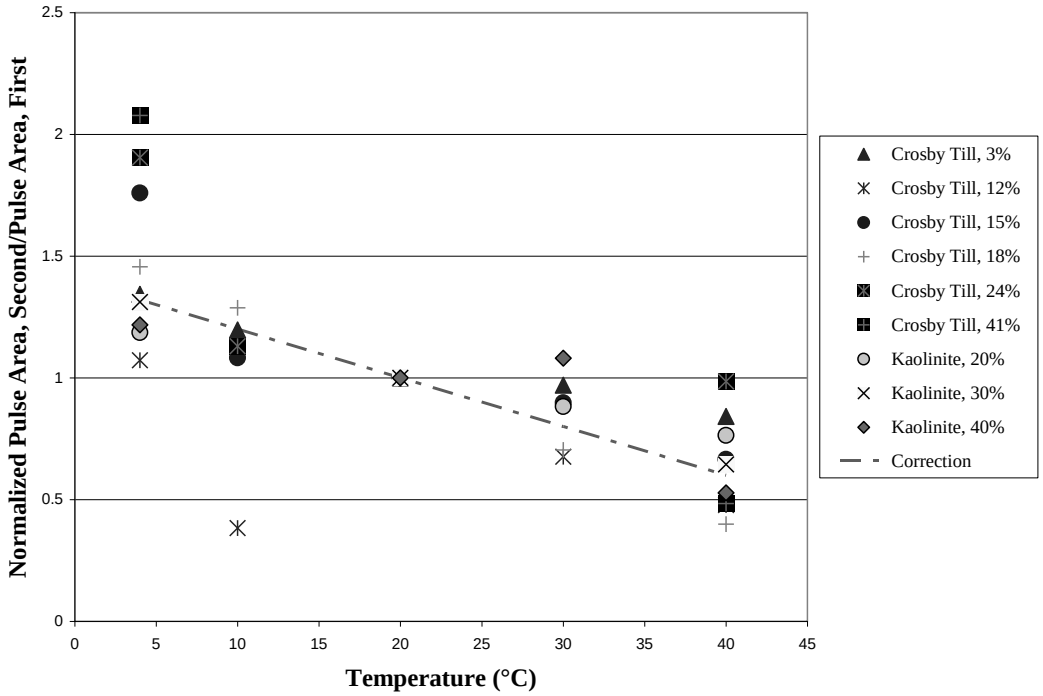

Figure 5-21 Normalized combined pulse area versus temperature with proposed correction for cohesive soils

The pulse area could be a valuable measurement used to analyze TDR waveforms in the future. The pulse area of the first reflection is fairly consistent for all of the soils tested. This implies that the pulse area of the first reflection is dependent on the probe head more than the soil type. This needs to be validated by testing alternate probe heads and comparing the resulting pulse areas. The temperature effects on the first pulse are minimal compared to the second pulse. This is illustrated when the pulse area of the second reflection is normalized by the pulse area of the first reflection. The temperature effects remain unchanged for cohesive soils. Increasing temperatures appear to have a more significant effect on cohesive soils than non-cohesive soils. The pulse area of the second pulse is more difficult to measure which caused significant scatter in the data. More refined methods for determining the pulse area of the second reflection are required.

CHAPTER 6. SUMMARY, CONCLUSIONS AND RECOMMENDATIONS

6.1. Summary and Conclusions

The focus of this study was to improve the accuracy of the time domain reflectometry method for measuring water content and dry density of soils. More reliable measurements of the apparent dielectric constant and electrical conductivity will improve the measurements of water content and dry density.

Different probe configurations were analyzed using finite difference and finite element analysis to determine geometric factors which are then used to calculate the electrical conductivity. It was shown that a finite element model based on groundwater flow principles can be used to determine the ratio of outer to inner conductor diameters for each probe configuration. These new ratios can help to improve consistency in measurements between the laboratory and the field which use different probe configurations.

Analysis of the temperature effects on the measured apparent dielectric constant and electrical conductivity of soils was performed on a previously acquired set of soils. Original analysis on the soils for temperature effects on K_a was performed and reported by Drnevich et al. (2001). Drnevich et al. (2001) manually analyzed the waveforms only for K_a. For this study the data were converted to a numerical file format and were analyzed for both K_a and EC_b using the PMTDR SM software developed by Yu (2003). A review of previous work on temperature effect on K_a reveals inconsistency in the reported trends. This study agrees with Drnevich et al. (2001) and Or and Wraith (1999), which observed that for cohesive soils the apparent dielectric constant increases with increasing temperature and decreases with increasing temperature for non-cohesive soils. Both the

Drnevich et al. (2001) and the proposed new correction can be used to correct measured values of the apparent dielectric constant for temperatures between 4°C and 40°C. The proposed correction has a smaller error than Drnevich et al. (2001) for the analyzed set of data. Correcting K_a for temperature is more critical for large variations in temperature.

Previous studies of the temperature effects on the electrical conductivity of soils do not report the same inconsistencies as with K_a. The trend reported, and also shown in this study, is that the electrical conductivity increases as temperature increases for all soil types. It was also noted that generally the measured electrical conductivity of soils can be corrected for temperature variations using a relationship established for the change in electrical conductivity of water with temperature. The proposed correction as a result of this study is also similar to the correction for water. There is still some error associated with the measured electrical conductivity possible caused by the water content of the soil. And a more thorough investigation of water content corrections is needed.

Zambrano (2006) proposed measuring the pulse area of the TDR waveform to use as a potential indicator of soil characteristics in addition to improving the estimations of water content and dry density. The data was analyzed for temperature effects of the pulse area of both the first and second reflections determined using the TDR Analysis software program developed by Murty Malladi. The effects of temperature on the pulse area of the first reflection are minimal compared to the second reflection. It is believed that the first reflection is largely influenced by the TDR device, cable and probe head and would be relatively constant for a given set of equipment. The pulse area of the second reflection is more difficult to accurately measure leading to scatter in the data. The trend generally shows that the pulse area decreases as temperature increases, but further investigation is needed before implementing the proposed correction factors.

6.2. Recommendations for Future Research

The focus of this study was to improve TDR measurements in soils through analysis of different probe head configurations and temperature effects. The following are

recommendations for future research which can help to improve the estimation of water content and dry density in soils using TDR.

1. Further development and testing of the TDR Analysis program should be performed. This could become a valuable tool for analyzing TDR waveforms accurately for apparent dielectric constants, electrical conductivities and pulse areas.

2. Evaluate the effects of water content on the electrical conductivity and try to incorporate corrections to improve the measurements.

3. Investigate the relationship between the pulse area of the first reflection and the TDR device, cable and probe head by comparing the pulse area for different equipment sets.

4. Establish a relationship between the pulse area of the second reflection and the apparent dielectric constant and the electrical conductivity. The pulse area of the second reflection is strongly influenced by the electrical conductivity of the soil. Soils with higher electrical conductivities tend to have smaller pulse areas due to a diminished response in the waveform at the second reflection. The first point used to measure the pulse area of the second reflection is approximately the same point used to calculate the apparent length of the waveform used to measure the apparent dielectric constant.

LIST OF REFERENCES

GeoStudio SEEP/W. GeoStudio 2004, Geo-Slope International.

Abu-Hassanein, Z. S., C. H. Benson, et al. (1996). "Electrical Resistivity of Compacted Clays." Journal of Geotechnical Engineering 122(5, May): 397-406.

Baker, J. M. and R. R. Allmaras (1990). "System for Automating and Multiplexing Soil Moisture Measurement by Time-Domain Reflectometry." Soil Science Society of America Journal 55: 1-6.

Becker, Rolf, Huebner, Christof and Stacheder, Markus, "Electromagnetic Simulation of Time Domain Reflectometry Probes: Simplified Approaches to Assess Calibration Curves, Sensitivity, Field Extent and Transient Response", Proc. TDR 2006, Purdue University, West Lafayette, USA, Sept. 2006, Paper ID 35, 17 p., https://engineering.purdue.edu/TDR/Papers

Benson, Craig H. and Wang, Xiaodong, "Temperature-Compensating Calibration Procedure for Water Content Reflectometers", Proc. TDR 2006, Purdue University, West Lafayette, USA, Sept. 2006, Paper ID 50, 16 p., https://engineering.purdue.edu/TDR/Papers

Bohn, H. L., J. Ben-Asher, et al. (1982). "Theories and Tests of Electrical Conductivity in Soils." Soil Science Society of America Journal 46: 1143-1146.

Drnevich, V. P., X. Yu, et al. (2001). “Temperature Effects on Dielectric Constant Determined by Time Domain Reflectometry.” TDR 2001 International Conference. Northwestern University, Evanston, Illinois.

Franson, M. A. H. (1985). Standard Methods for the Examination of Water and Wastewater. , Am. Public Health Assoc., Washington, D.C.

Friedman, S.P., S.B. Jones and D. A. Robinson, “Plenary Lecture: Review of Geometrical and Interfacial Factors Determining the Effective Permittivity-Volumetric Water Content Relationships of Soils and Rocks”, Proc. TDR 2006, Purdue University, West Lafayette, Sept. 2006.

Giese, K. and R. Tiemann (1975). "Determination of the complex permittivity from a thin sample time-domain reflectometry, improved analysis of the step response waveform." Adv. Molec. Relax. Processes 7: 45-59.

Heimovaara, T. J., A. G. Focke, et al. (1995). "Assessing Temporal Variations in Soil Water Composition with Time Domain Reflectometry." Soil Science Society of America Journal 59: 689-698.

Hook, W. R. and N. J. Livingston (1995). "Propagation Velocity Errors in Time Domain Reflectometry Measurements of Soil Water." Soil Science Society of America Journal 59: 92-96.

Krahn, J. (2004). Seepage Modeling with SEEP/W An Engineering Methodology, GEO-SLOPE International, Ltd.

Ledieu, J., P. De Ridder, et al. (1986). "A Method of Measuring Soil Moisture by Time-Domain Reflectometry." Journal of Hydrology 88(3-4): 319-328.

Lesmes, D. P. and S. P. Friedman (2005). Electrical and Hydrogeological Properties. Hydrogeophysics. Dordrecht, The Netherlands, Springer.

Lin, C. P., C. C. Chung, et al. (2006). "Devlopment of TDR Penetrometer Through Theoretical and Laboratory Investigations: 2. Measurement of Soil Electrical Conductivity." Geotechnical Testing Journal 29(4).

Lin, C. P., H. Tang, et al. (2006). "Development of TDR Penetrometer Through Theoretical and Laboratory Investigations: 1. Measurement of Soil Dielectric Permittivity." Geotechnical Testing Journal 29(4).

Mualem, Y. and S. P. Friedman (1991). "Theoretical Prediction of Electrical Conductivity in Saturated and Unsaturated Soil." Water Resources Research 27(10): 2771-2777.

Nadler, A. (1982). "Estimatin the Soil Water Dependence of the Electrical Conductivity Soil Solution/Electrical Conductivity Bulk Soil Ratio." Soil Science Society of America Journal 46: 722-726.

Or, D. and J. M. Wraith (1999). "Temperature Effects on Soil Bulk Dielectric Permittivity Measured by Time Domain Reflectometry: A physical model." Water Resources Research 35(2): 371-383.

Pepin, S., N. J. Livingston, et al. (1995). "Temperature-Dependent Measurement Errors in Time Domain Reflectometry Determinations of Soil Water." Soil Science Society of America Journal 59: 38-43.

Persson, M. and R. Berndtsson (1998). "Texture and Electrical Conductivity Effects on Temperature Dependency in Time Domain Reflectometry." Soil Science Society of America Journal 62(887-893).

Rhoades, J. D., Raats, P.A.C., and Prather, R.J. (1976). "Effects of Liquid-phase Electrical Conductivity, Water Content, and Surface Conductivity on Bulk Soil Electrical Conductivity." Soil Science Society of America Journal 40: 651-655.

Rinaldi, V. A. and G. A. Cuestas (2002). "Ohmic Conductivity of a Compacted Silty Clay." Journal of Geotechnical and Geoenvironmental Engineering 128(10): 824-835.

Robinson, D. A., S. B. Jones, et al. (2003). "A Review of Advances in Dielectric and Electric Conductivity Measurement in Soils Using Time Domain Reflectometry." Vadose Zone Journal 2: 444-475.

Robinson, R. A. and R. H. Stokes (1959). Electrolyte Solutions, Butterworths, London. pp. 476-470.

Siddiqui, S. I., V. P. Drnevich, et al. (2000). "Time Domain Reflectometry Development for Use in Geotechnical Engineering." Geotechnical Testing Journal 23(1): 9-20.

Strogryn, A. (1971). "Equations for calculating the dielectric constant of saline water." IEEE Trans. Microwave Theory Tech. 19: 733-736.

Timlin, D. J. and Y. A. Pachepsky (1996). "Comparison of Three Methods to Obtain the Apparent Dielectric Constant from Time Domain Reflectometry Wave Traces." Soil Science Society of America Journal 60: 970-977.

Topp, G. C., J. L. Davis, and A. P. Annan (1980). "Electromagnetic Determination of Soil Water Content: Measurements in Coaxial Transmission Lines." Water Resources Research 16(3): 574-582.

Ulaby, F. T., R. K. Moore, et al. (1986). Microwave Remote Sensing: Active and Passive, From Theory to Applications. Norwood, Mass., Artech House. pp. 456.

Weast, R. C., Ed. (1986). CRC Handbook of Chemistry and Physics. Boca Raton, Forida, CRC Press.

Wraith, J. M. and D. Or (1999). "Temperature Effects on Soil Bulk Dielectric Permittivity Measured by Time Domain Reflectometry: Experimental Evidence and Hypothesis Development." Water Resources Research 35(2): 361-369.

Yu, X. (2003). Influence of Material Properties and Environmental Conditions on Electromagnetic Wave Propagation in Soil. West Lafayette, IN, Purdue University. Doctor of Philosophy. pp. 109-118.

Yu, X. and V. P. Drnevich (2004). "Soil Water Content and Dry Denstiy by Time Domain Reflectometry." Journal of Geotechnical and Geoenvironmental Engineering 130(9): 922-934.

Zambrano, C. E. (2006). Soil Type Identification Using Time Domain Reflectometry. Civil Engineering. West Lafayette, IN, Purdue University. Master of Science in Civil Engineering. pp. 69, 114-155.

LIST OF REFERENCES